



저작자표시-비영리-변경금지 2.0 대한민국

이용자는 아래의 조건을 따르는 경우에 한하여 자유롭게

- 이 저작물을 복제, 배포, 전송, 전시, 공연 및 방송할 수 있습니다.

다음과 같은 조건을 따라야 합니다:



저작자표시. 귀하는 원저작자를 표시하여야 합니다.



비영리. 귀하는 이 저작물을 영리 목적으로 이용할 수 없습니다.



변경금지. 귀하는 이 저작물을 개작, 변형 또는 가공할 수 없습니다.

- 귀하는, 이 저작물의 재이용이나 배포의 경우, 이 저작물에 적용된 이용허락조건을 명확하게 나타내어야 합니다.
- 저작권자로부터 별도의 허가를 받으면 이러한 조건들은 적용되지 않습니다.

저작권법에 따른 이용자의 권리는 위의 내용에 의하여 영향을 받지 않습니다.

이것은 [이용허락규약\(Legal Code\)](#)을 이해하기 쉽게 요약한 것입니다.

[Disclaimer](#)

Thesis for the Degree of Master of Engineering

**Controller Design for Automatic
Diameter-Adjusting and Driving of a
Wheel Type Pipe Inspection Robot**

by

Husam Hasan Khudhair

**Department of Mechanical Design Engineering,
The Graduate School,
Pukyong National University**

February 2016

Controller Design for Automatic Diameter-Adjusting and Driving of a Wheel Type Pipe Inspection Robot

**바퀴형 관로검사로봇의 직경조정 및
주행제어용 제어기 설계**

by

Husam Hasan Khudhair

Advisor: Professor Sang Bong Kim

**A thesis submitted in partial fulfillment of the requirements
for the degree of Master of Engineering**

**In the Department of Mechanical Design Engineering,
The Graduate School,
Pukyong National University**


February 2016

Controller Design for Automatic Diameter- Adjusting and Driving of a Wheel Type Pipe Inspection Robot

A thesis

By HUSAM HASAN KHUDHAIR

Approved as to styles and contents by:





(Chairman) Gi Sik Byun



(Member) Yeon Wook Choe



(Member) Sang Bong Kim

December, 2015

Acknowledgements

‘No Herculean task can be consummated without the support and contribution of a number of individuals and that is the very first essence of success of any colossal work.’ Here I take the opportunity to express my gratitude toward all those who helped me directly and indirectly to complete my studies in Republic of Korea.

Initially, I would like to humble myself toward Allah SWT, the Loving and Merciful Lord. Because of His grace and help, I can carry on my study in Republic of Korea properly.

Firstly, I would like to express my deep gratitude to my professor, Professor Sang Bong Kim, who has helped me significantly in completing my Master program. I really appreciate his kindness and helps that he has shown to me during my study in his excellent laboratory.

I would also like to express my sincere gratitude to the members of my thesis committee, Professor Gi Sik Byun, Professor Yeon Wook Choe and Professor Sang Bong Kim, for their helpful comments and suggestions for my thesis.

Furthermore, I would like to express my profound gratitude to Professor Hak Kyeong Kim for his great help and advice to finish my research and my master thesis very well.

I would also like to express my gratitude to all members of Computer Integrated Manufacturing Electronics Commerce (CIMEC) laboratory for their cooperation and for all the kindness and friendship. Dr. Pandu Sandi Pratama, Dr. Phuc Thinh Doan, Mr .Van Tu Duong, Mr. Nguyen Trong Hai, Mr. Hung Nguyen Huy as Doctor

course students, Mr. Jin Wook Kim, Mr Xing Kun Ding, Mr. Sheng Dongbo, Mr. Jae Hoon Jeong, Mr. Tian Shui Gao as Master course students, and Mr .Jin Il Kim and Jeong Woong Lee as Undergraduate students.

I would also like to express my gratitude to Korean government , Iraqi government and my dear Wassit province to support for me. Last but not least, I would like to express my deepest gratitude to all members of my family, my father, my mother, my dear wife Makarem who has endured a lot in my success, my kids, Dhai, Fawatim, Mohammed, Yousif, my brothers, Husham, Basam, my Uncle Abo Tayef, my Aunt Om Tayef and all my relatives for their love, endless prayers, encouragement and support for me not only in completing Master program but also in the whole of my life.

Pukyong National University, Busan, Korea

November, 2015

Husam Hasan Khudhair

Contents

Acknowledgements	i
Contents	iii
Abstract.....	vi
List of Figure	ix
List of Tables	xiv
Chapter 1. Introduction.....	1
1.1. Background and motivation.....	1
1.2. Problem statements	10
1.3. Objective and research method	12
1.4. Outline of thesis and summary of the contribution.....	13
Chapter 2. System Description and Modeling.....	16
2.1. System description	16
2.2. System modeling.....	21
2.2.1. Diameter adjusting modeling.....	21
2.2.2. Driving speed modeling.....	25
Chapter 3. Driving Algorithm.....	30
3.1. Curved pipe	30
3.2. Simulation results in curved pipe.....	33
Chapter 4. Controller Design	40
4.1. Diameter tracking controller design.....	40
4.1.1. PI Controller.....	40
4.1.2. Fuzzy Controller	41

4.2.	Driving Controller.....	44
4.2.1.	PI Controller.....	44
4.2.2.	Fuzzy Controller	44
Chapter 5.	Controller Implementation	48
5.1.	Hardware Architecture.....	48
5.2.	Electrical part design.....	50
5.2.1.	Expansion DC motor.....	51
5.2.2.	Microcontrollers AVR ATmega8 and ATmega128 ...	52
5.2.3.	Motor driver.....	54
5.2.4.	Ultrasonic sensor.....	54
5.2.5.	Driving DC motor	55
5.2.6.	Angle sensor.....	56
5.2.7.	Camera sensor	57
5.3.	Proposed control system	57
5.4.	Control process	60
5.4.1.	Universal joint.....	63
5.4.2.	Battery	64
Chapter 6.	Simulation and Experimental Results.....	65
6.1.	Simulation results using the proposed diameter tracking controllers	65
6.2.	Simulation results using the proposed driving controllers	69
6.3.	Experimental results for driving control	78
6.4.	Driving test result using the fuzzy logic controller.....	89

Chapter 7. Conclusions.....	90
7.1. Conclusions.....	90
7.2. Future Works	94
References.....	95
Publications and Conferences.....	100



Controller Design for Automatic Diameter-Adjustable and Driving of a Wheel Type Pipe Inspection Robot

Husam Hasan Khudhair

**Department of Mechanical Design Engineering,
The Graduate School, Pukyong National University**

Abstract

Recently, various pipeline inspection robots have been researched. However, there are few control methods of the pipeline inspection robots (PIRS). Therefore, a few control methods of the pipeline inspection robot are needed.

This thesis proposes a controller design for a wheeled type of pipe inspection robot to adjust its diameter atomically and drive inside the pipelines with diameters from 300 to 500 mm using fuzzy logic control. The developed pipeline inspection robot can be used to inspect the sea-water in pipelines. To do this task, the followings are done. Firstly, mechanical design of a wheel type pipe inspection robot is proposed. The proposed PIR consists of driving part and sensor part. The driving part is composed of two modules and universal joint: passive module and active module that produces pressing force and universal joint connecting them. The sensor part is composed of ultrasonic sensors, angle sensor and camera sensor. Ultrasonic sensors are used for detecting curvature of pipe line and wheel positions, whereas the camera sensor is used for detecting the inside of the pipeline obtaining its inner state data in real time. Both

the active and passive modules consist of a body, 3 driving modules and 3 4-bar linkage that are spaced at an angle 120 each other. The 4-bar linkages in the active and passive modules are extended and shrunk by expansion DC motor and compression spring, respectively. Each driving module of the proposed PIR consists of driving wheel DC motor, motor case, double type wheel, and is connected to the 4-bar linkage. The body of the active module consists of front body, rear body, rotating thread shaft, gear motor and expansion DC motor, whereas the body of the passive module consists of front body, rear body, spring and shaft. Secondly, for system modeling of the active module, kinematic modeling of 4-bar linkage of the proposed PIR and dynamic modeling of the expansion DC motor to track the reference diameter are proposed. In addition, kinematic modelings of the proposed PIR are proposed and dynamic modelings of the driving DC motor for driving inside the pipelines are proposed. Thirdly, a driving algorithm for driving the proposed PIR in a curved pipelines and straight pipelines is proposed. This driving algorithm is used to design reference wheel velocities and reference PIR linear velocity by detecting curvatures of curved pipelines, straight pipelines and wheel position depending on the posture of the proposed PIR using 3 ultrasonic sensors for the curve pipeline and 2 ultrasonic sensors to the straight pipeline. Fourthly, a conventional proposed PI controller and a fuzzy logic controller based on the kinematic modeling of the 4-bar linkage and the dynamic modeling of expansion the DC motor are designed for the proposed PIR to track given reference diameters of pipelines with different diameters by making the tracking errors. Fifthly, based on the kinematic modeling and the dynamic modeling of the driving wheel DC motor of the PIR, a conventional PI

controller and a fuzzy logic controller are designed to track the wheel reference velocities and the reference PIR linear velocity obtained from the proposed drive algorithm in order to drive well in the curved pipeline with different diameters. Sixthly, a control system using computer, ATmega8 microcontroller, RS232 communication channel, ultrasonic sensors, camera, and angle sensor is developed for the proposed PIR to track the reference diameter and reference wheel velocities and reference PIR linear velocity in order to move along the wall of the pipeline. Finally, the simulation and experimental results are shown that the proposed fuzzy logic controllers make PIR track the reference diameter and drive with the reference wheel velocities and the reference PIR linear velocity inside a given pipeline better than the conventional PI controllers. To prove the effectiveness and the applicability of the designed driving algorithm and the proposed controllers during driving experimental results of the proposed PIR in the pipeline, detected images of the pipeline wall are obtained from camera sensor.

Keywords: Pipe inspection robot, 4-bar linkage, Fuzzy logic control, Automatic diameter controller.

List of Figure

Fig. 1.1 Corrosion of pipeline	1
Fig. 1.2 Manual inspection and maintenance of pipe	2
Fig. 1.3 Classification of pipe inspection robot	2
Fig. 1.4 Wall press type pipe inspection robot.....	5
Fig. 1.5 Pipe inspection robot using tension spring	6
Fig. 1.6 Collaboration type pipeline inspection robot.....	7
Fig. 1.7 Screw drive in-pipe robot	7
Fig. 1.8 Earth worm type in-pipe robot.....	9
Fig. 1.9 Tube crawling type pipe inspection robot	9
Fig. 2.1 Design of a wheeled type pipe inspection robot used for this thesis	17
Fig. 2.2 Structure of the active module.....	18
Fig. 2.3 Side view of the active module.....	18
Fig. 2.4 Structure of the passive module.....	19
Fig. 2.5 Universal joint	20
Fig. 2.6 Structure of the driving module.....	20
Fig. 2.7 Mechanical system of the proposed pipe inspection robot.	23
Fig. 2.8 DC explanation motor system	24
Fig. 2.9 Coordinate frame of the proposed pipe inspection robot....	26
Fig. 3.1 Driving principle of in-pipe inspection robot	30
Fig. 3.2 Position of wheels in curved PIR.....	31
Fig. 3.3 Distance between sensor and pipeline	31
Fig. 3.4 Relation between ω_{wiref} and R_i	33
Fig. 3.5 In-pipe inspection robot in curved pipe	34
Fig. 3.6 Values of I_p , I_q , I_r in $\phi 300$ mm.....	34

Fig. 3.7 Values of I_p, I_q, I_r in $\phi 500$ mm.....	35
Fig. 3.8 Values of R_p, R_q, R_r in $\phi 300$ mm	35
Fig. 3.9 Values of R_p, R_q, R_r in $\phi 500$ mm	36
Fig. 3.10 Values of V_p, V_q, V_r in $\phi 300$ mm	37
Fig. 3.11 Values of V_p, V_q, V_r in $\phi 500$ mm	37
Fig. 3.12 Values of $\omega_p, \omega_q, \omega_r$ in $\phi 300$ mm	38
Fig. 3.13 Values of $\omega_p, \omega_q, \omega_r$ in $\phi 500$ mm	38
Fig. 3.14 Flow chart of the proposed driving algorithm	39
Fig. 4.1 Block diagram of the conventional PI controller.....	40
Fig. 4.2 Membership function for input e_h	41
Fig. 4.3 Membership function for input \dot{e}_h	41
Fig. 4.4 Membership function of output u	42
Fig. 4.5 Block diagram of the proposed fuzzy logic controller for this thesis	43
Fig. 4.6 Block diagram of the conventional PI controller.....	44
Fig. 4.7 Membership function for input $e_{\theta i}$	45
Fig. 4.8 Membership function for input $\dot{e}_{\theta i}$	45
Fig. 4.9 Membership function of output u_{di}	46
Fig. 4.10 Block diagram of the proposed fuzzy logic controller for this thesis	47
Fig. 5.1 Wireless camera VIJE IP-2000 PTW	48
Fig. 5.2 Collaborative structure between two modules.....	49
Fig. 5.3 Flow chart of the proposed control system.....	50
Fig. 5.4 Developed in-pipe inspection robot.....	50

Fig. 5.5 Electrical part design of the proposed pipe inspection robot..	51
Fig. 5.6 Expansion DC motor	51
Fig. 5.7 Microcontroller Part.....	52
Fig. 5.8 Microcontroller AVR ATmega128.....	53
Fig. 5.9 Motor driver.....	54
Fig. 5.10 Ultrasonic sensor SRF-10.....	55
Fig. 5.11 Driving motor IG-32RGM 05 Type	55
Fig. 5.12 Angle sensor gaussmakov B10kΩ.....	56
Fig. 5.13 Camera sensor.....	57
Fig. 5.14 Schematic block of the proposed control system	58
Fig. 5.15 Graphic user interface.....	61
Fig. 5.16 Ultrasonic sensor and camera sensor.....	61
Fig. 5.17 Control panel for manual operation.....	62
Fig. 5.18 Universal joint	64
Fig. 5.19 Lithium polymer battery	64
Fig. 6.1 Output radius h_i of the proposed PIR using both diameter tracking controllers	67
Fig. 6.2 Radius error e_h using the proposed PIR using both diameter tracking controllers	68
Fig. 6.3 Control input u of the proposed PIR using both diameter tracking controllers	68
Fig. 6.4 Pipeline for simulation and experiment.....	69
Fig. 6.5 Elbow and pipe specification (mm).....	70
Fig. 6.6 Angular velocity of the proposed PIR with respect to x axis	73

Fig. 6.7 Angular velocity error of the proposed PIR with respect to x axis	74
Fig. 6.8 Angular velocity of the proposed PIR with respect to y axis	74
Fig. 6.9 Angular velocity error of the proposed PIR with respect to y axis	75
Fig. 6.10 Linear velocity of the proposed PIR	75
Fig. 6.11 Linear velocity error of the proposed PIR	76
Fig. 6.12 Wheel angular velocities	76
Fig. 6.13 Wheel angular velocity error $e_{\theta 1}$	77
Fig. 6.14 Wheel angular velocity error $e_{\theta 2}$	77
Fig. 6.15 Wheel angular velocity error $e_{\theta 3}$	78
Fig. 6.16 Experimental angular velocity of the proposed PIR with respect to x axis	80
Fig. 6.17 Experimental angular velocity error of the proposed PIR with respect to axis	80
Fig. 6.18 Experimental angular velocity of the proposed PIR with respect to y axis	81
Fig. 6.19 Experimental angular velocity error of the proposed PIR with respect to y axis	82
Fig. 6.20 Experimental linear velocity of the proposed PIR	83
Fig. 6.21 Experimental linear velocity error of the proposed PIR	84
Fig. 6.22 Experimental wheel angular velocities	84
Fig. 6.23 Experimental wheel angular velocities error $e_{\theta 1}$	85
Fig. 6.24 Experimental wheel angular velocities error $e_{\theta 2}$	85
Fig. 6.25 Experimental wheel angular velocities error $e_{\theta 3}$	86
Fig. 6.26 Experimental ultrasonic sensor data (I_p , I_q , I_r)	87

Fig. 6.27 Driving experiments in the pipeline	88
Fig. 6.28 Images of the pipeline state taken by the camera sensor during driving test	89



List of Tables

Table 1.1	Specification of a wall press type pipe inspection robot..	5
Table 1.2	Specification of the screw drive-pipe robot	8
Table 2.1	Specification of the pipe inspection robot used for this thesis.....	21
Table 2.2	Nomenclature of linkage and expansion DC motor	21
Table 4.1	Fuzzy rules	42
Table 4.2	Fuzzy rules	46
Table 5.1	Specification of expansion DC motor IG-52 GM 03 Type	52
Table 5.2	Specification of microcontroller AVR ATmega8	52
Table 5.3	Specification of microcontroller AVR ATmega128	53
Table 5.4	Specification of motor drive	54
Table 5.5	Specification of ultrasonic sensor	55
Table 5.6	Specification of driving DC motor.....	56
Table 5.7	Specification of angle sensor	56
Table 5.8	Specification of camera sensor	57
Table 5.9	Configuration of the propose control system	58
Table 5.10	Specification of battery	64
Table 6.1	Parameters and initial values of the i^{th} expansion DC motor	65
Table 6.2	Parameters and initial values.....	69

Chapter 1. Introduction

1.1. Background and motivation

Pipelines are widely used to carry natural gas and oil to destinations. They range from high-pressure transmission lines to low-pressure distribution lines in order to prevent a failure/leakage in a pipeline due to corrosion and/or high pressure as shown in Fig. 1.



Fig. 1.1 Corrosion of pipeline

The interiors of the pipes need to be routinely monitored and inspected to evaluate the need to maintain or repair the pipeline and to decide the most effective means to do so. Cutting one or more samples of the pipe and inspecting them manually is one of the most common methods used for diagnosing a pipeline. This manual inspection method shown Fig. 1.2 and needs high cost and a long time [1, 2]. Moreover, this method also does not provide comprehensive information about the status of the whole pipe because of the variations in corrosion rate found in different sections of a pipe.



Fig. 1.2 Manual inspection and maintenance of pipe

Since space availability is one of the challenges that face in-pipe robots [3], many concepts have been adopted to tackle this challenge and resulted in developing different kinds of in-pipe robots shown as Fig. 1.3 such as pig type (a), wheel type (b), caterpillar type (c) wall-press type (d), walking type (e), inchworm type (f) and screw type (g) and combined types [3-27].

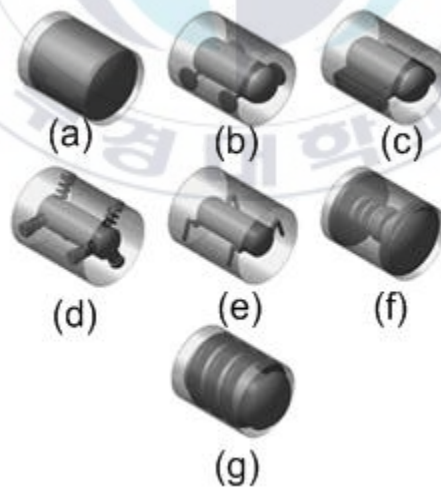


Fig. 1.3 Classification of pipe inspection robot

Moreover, pipe diameters vary by the usage and flow conditions of the pipes, hence another main challenge that may pose technical difficulties to pipe inspection robot (PIRS) is the ability to navigate inside a pipe of changing diameter a pipe comprising segments of different diameters. This challenge becomes more difficult when the change in pipe diameter is 1) in step (not smooth) and 2) in considerably large diameter change e.g, more than double the smaller section. In these scenarios, when the robot passes from a larger pipe to a smaller pipe diameter vice versa, it has to be able to: a) find the hole location at the cross-section where the pipes mate (e.g. up, down, right or left of the center of the hosting pipe segment); b) steer into the hole direction; c) change its radial dimension to negotiate the receiving pipe diameter; and d) propel/move autonomously forward and backward in a limited and constrained space. Several concepts of PIRs have been developed to move through a pipeline with propulsion mechanisms that depended on friction force which might not be always sufficient to cause the linear motion [4-9]. However, the steering control has not been emphasized. Other mechanisms were designed to overcome those difficulties by utilizing sets of front and rear rollers/wheels which are pushed against the interior wall of the pipe and used to drive the robot [10-15]. Although some of those PIRs could travel only in pipes of constant diameters [10-11], others could handle only small changes in pipe diameters since their wheels were pushed radially against the pipe walls using compression springs of small strokes because springs usually exerted smaller forces towards the end of the spring stroke causing slipping of the wheels [12-17]. One notable example on a PIR that could adapt to large changes in pipe diameters

was [15], which could handle a pipe change of 400-700 mm. It used 3 pantograph mechanisms distributed radially at 120 degrees to push the wheels against the pipe. Moreover, inch-worm robots [18-20] and snake-like robots [21-23] utilized a serpentine motion to travel through horizontal and curved pipes, but their designs allowed limited radial and axial extension-contraction to provide clamping force against pipe walls. Also, pipe crawlers demonstrated good ability in dealing with the change in pipe diameters [24-25]. In spite of the advanced designs of those robots, their intricate designs showed deficiencies in meeting one or more of the intended tasks when they navigated through a pipeline, especially, in dealing with sudden changes of pipe diameter.

A wall-press type pipe inspection robot as shown in Fig. 1.4 was proposed in [4-9]. This robot had three pantograph type links spaced in 120° with three caterpillar track wheels for the adaptation to pipe diameter with the wall-pressing force adjustment using DC motor and its specification was shown in Table 1.1. The pipe inspection robot consisted of driving module and control module. The control of the pipe inspection robot was considered as a mass-spring-damper-system. The dynamic model of the system was obtained by process model identification method. An observer was designed to estimate the unknown wall-pressing force to sustain the pipe inspection robot in pipeline. An algorithm of wall-pressing force generator was presented to find out an appropriate wall-pressing force when the appropriate wall-pressing force was given as a reference value of wall-pressing force, and PD controller was designed to make the estimated wall-pressing force track the reference wall-pressing force irrelatively to variable diameter of pipeline.

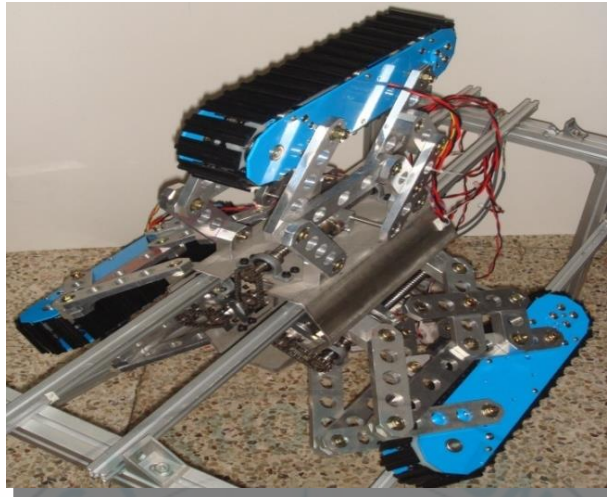


Fig. 1.4 Wall press type pipe inspection robot

Table 1.1 Specification of a wall press type pipe inspection robot

Item	Length of Robot	Weight of Robot	Variable dimension
Value	0.45m	30kg	0.53m~0.88m

The pipe inspection robot using tension spring, MRINSPECT, for a long-distance inspection of pipelines as shown in Fig. 1.5 was developed S. R. Roh et al. [29]. This robot system was PIRs using tension spring. The systems had outstanding mobility and several characteristic features, which made it possible to apply the proposed systems in pipelines with complicate geometries regardless of the effect of gravity, its postures, and the direction of moving. However, the mechanism of the in-pipe robot should be adaptable to the characteristic condition of the pipelines because of using tension spring.



Fig. 1.5 Pipe inspection robot using tension spring

Fig. 1.6 showed collaboration type PIR with two modules. It was developed by Y. S. Kwon et al. and could inspect 90-100m pipelines [30]. Each robot module consisted of three pairs, and each pair was operated by a micro-dc motor. Independent control of the speed of each caterpillar wheel chain (CWC) allowed steering capability passing through elbows or T-branches, and the CWC was foldable by using an embedded four-bar mechanism and a compression spring. This PIR could adjust its diameter and contact the inner wall of pipelines with an irregular cross-sectional area. This PIR also overcome the sharp corners of branches and elbows. The motion of this PIR was equivalent to an unidirectional mobile robot in steering at corners of an elbow or T-branch. However, this PIR had disadvantage in motion of pipeline, because of its depended on of force spring of different diameter.

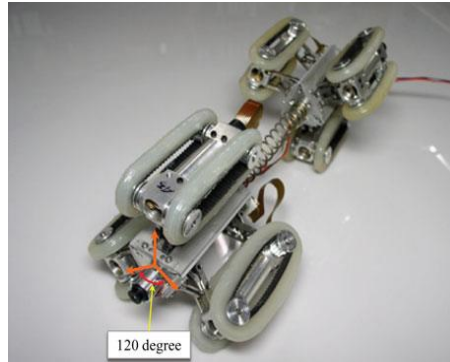


Fig. 1.6 Collaboration type pipeline inspection robot

A screw driver in-pipe robot as shown in Fig. 1.7 was developed by A. Kakogawal et al. [31]. The system enabled the robot to navigate through the bent pipe and T-branch using only two actuators. The robot has three modes of locomotion such as screw driving, steering, and rolling which enable it to navigate through T -branches. The validity of this mechanism was tested by performing experiments in various types of pipelines. According to the results, the robot could pass through all horizontal pipes. However, the pathway selection mechanism had disadvantage in mobility. Because one output occasionally transmitted to another output, it caused unexpected motions.

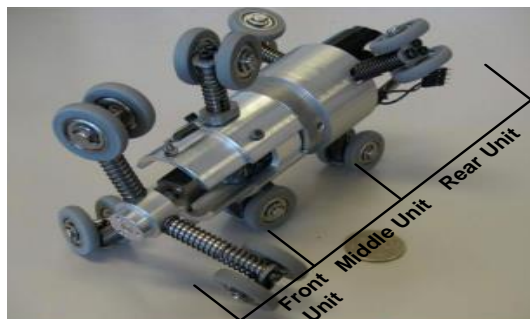


Fig. 1.7 Screw drive in-pipe robot

The robot could not navigate through all pipelines, especially, vertical pipes and branch pipes. Its specification is listed in Table 1.2.

Table 1.2 Specification of the screw drive-pipe robot

Item	Value/[Unit]
Axial Length	175.8 [mm]
Wheel Diameter	109[mm]
Degree of the Wheel	10 [deg]
Max Velocity	500 [mm/s]
Total Weight	0.35[kg]

Fig. 1.8 showed an artificial earthworm type PIR developed by M. Ono et al. [32] and was constructed by three bellows, friction rings and three electromagnetic valves. This robot could move in the pipe which had 8 elbows and was $\phi 79$ mm in inner diameter and 32 m in length. The traction force depended on the number of friction rings. The increasing to 20 friction rings may be able to move more than 40 m. The robot showed feasibility as an in-pipe inspection robot of the primary cooling-water pipe of atomic power plant transparent vinyl chloride. The "U" letter curving pipe connected with double elbows is 1.5 m in length and 300 mm in radius of curvature. Consequently, the robot could not pass the elbows when the robot moved to vertical direction.

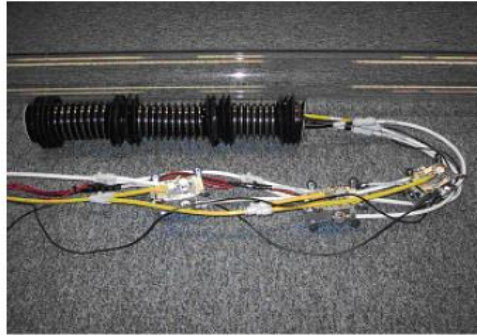


Fig. 1.8 Earth worm type in-pipe robot

Fig. 1.9 showed a tube crawling type PIR, MORLTZ, developed by A. Zagler [33]. Its improvements in climbing through tube junctions were presented. It was able to move with a legged locomotion through pipes of any inclination and bore its weight only with friction forces. The robot had four new joints in the central body which allowed to rotate in the pipe and to bend its body. The gait pattern that was used to walk through a pipe was presented and a simulation results were shown to describe this movement. However, this robot needs at least three actuators for each leg. Moreover, the actuators used were still heavy compared to their power output. This makes the robots very heavy or weak if they have many legs.

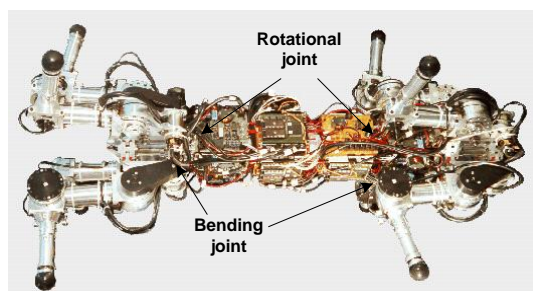


Fig. 1.9 Tube crawling type pipe inspection robot

Many pipe inspection robots have been developed in recent years, but the steering control has not been emphasized. In [34], trajectory tracking control for pipe inspection robot was proposed using PID controller. However, PID controllers are significantly limited in their capabilities for the nonlinear system because the desired transient performances in the closed-loop system cannot be guaranteed in the presence of nonlinear plant with parameter variations and unknown external disturbances. In [35], flatness-based controller was proposed to track the trajectory. However, since flat system is linearized by exact feedback linearization, it is less robust against parametric uncertainties and measurement noise. In [36], the robot can be easily controlled using GUI on a PC. A stable and smooth fuzzy steering controller for operating inside the pipes is constructed. However, the fuzzy steering controller was only a steering controller without controlling diameter. In [37], trajectory tracking control for the pipe inspection robot was proposed using optimal LQR controller. However, LQR controllers are significantly limited in their capabilities since the system is nonlinear. The desired transient performances of LQR controller in the closed-loop system cannot be guaranteed in the presence of nonlinear plant parameter variations and unknown external disturbances. To solve these problems, a new controller must be needed.

1.2. Problem statements

To inspect pipelines, a wheel type pipe inspection robot must have ability to navigate inside variable diameter pipelines such as a pipe with segments of different diameters.

To drive inside a pipeline with different diameters, the following two controllers must be developed. One is a diameter tracking controller used for adjusting diameters of the proposed PIR to given reference diameters, another is a driving controller used to track given reference wheel angular velocities and reference PIR linear velocity in pipeline.

The problem statement is to design the two controllers for a wheel type pipe inspection robot as follows:

- To design and manufacture a wheel type pipe inspection robot suitable to drive inside a pipeline with different diameters, elbows and straight pipe line.
- To get modelings for designing two controllers.
- To design two controllers to adjust the diameter of the designed PIR to reference diameters and for the proposed PIR to track inside reference wheel velocities and reference PIR linear velocity inside pipeline with a different diameters , elbows and straight pipelines.

To developed a control system to implement the proposed two controllers:

- To perform the simulation and experiment for evaluating results of the proposed driving algorithm and controllers.

1.3. Objective and research method

The objective of this thesis is to propose a diameter tracking controller for adjusting the diameter of the proposed PIR to given reference diameters and a driving controller for the wheel type inspection robot (PIR) to track reference wheel angular velocities and reference PIR linear velocities in various pipelines. To do these tasks, the following steps are executed. Firstly, a wheel type pipe inspection robot that can work in pipelines with 150 to 250 mm in radius is developed. The robot consists of two modules and universal joint: active module and passive module such that each module has three wheel configurations with different mechanism to expand and shrink wheels, and universal joint. Secondly, kinematic modelings of 4-bar linkage of the proposed PIR and dynamic modelings of the expansion DC motor and the driving wheel DC motor are proposed. Thirdly, a driving algorithm for driving the robot in a curved pipeline and straight pipeline is proposed. This driving algorithm is used to design wheel reference velocities and PIR reference velocities by detecting curvatures of the curved pipeline and the straight pipeline and wheel position depending on the posture of the proposed PIR obtained using 3 ultrasonic sensors for the curve pipeline and 2 ultrasonic sensors for straight pipeline. Fourthly, based on the kinematic modeling of the 4-bar linkage and the dynamic modeling of the expansion DC motor, a conventional PI controller and a fuzzy logic controller are designed for the proposed PIR to track its given reference diameter. Fifthly, based on the kinematic modeling of the proposed PIR and the dynamic modeling of its driving wheel DC motor, a conventional PI controller and a fuzzy controller are designed to track the wheel reference velocities and reference PIR linear velocity obtained from

the proposed driving algorithm in order to drive well in the curved pipeline and the straight pipeline in different diameter pipe with multiple elbows. Sixthly, for implementation of the designed controllers, a control system using computer, ATmega8 microcontroller, RS232 communication channel, ultrasonic sensors, camera, and angle sensor for driving the proposed PIR is developed for automatically adjusting its diameter to the reference diameters and wheel reference velocities and its reference PIR linear velocity in order to move along the wall of the pipeline. Finally, the simulation and experimental results show the proposed two controllers can work very well by making the proposed PIR track the reference wheel velocities and reference diameter in horizontal straight pipelines, elbow pipelines and different diameter pipelines to show their effectiveness and the applicability.

1.4. Outline of thesis and summary of the contribution

Chapter 1: Introduction

In this chapter, firstly, background and motivation of this thesis are presented. Secondly, problem statements of this thesis are described. Thirdly, the objective and research method of this thesis are then described. Finally, the outline of thesis and summary of the contributions is described.

Chapter 2: System Description and Modeling

This chapter describes the structure of the proposed inspection pipeline robot and its modelings. To do these tasks, the followings are done. First, kinematic modelings of the 4-bar linkage and the proposed pipeline inspection robot and dynamic modelings for the expansion DC motor and the driving DC motor are proposed.

Chapter 3: Driving Algorithm

This chapter proposed a smooth driving algorithm for the proposed pipe inspection robot in curve pipe with the target rotation angular velocity of the wheel from the driving algorithm to determine a target speed of the pipe inspection robot.

Chapter 4: Controller Design

This chapter proposes a conventional PI control and a fuzzy logic controller to track reference diameters and to track the reference wheel velocities and the reference PIR linear velocity obtained by the proposed driving algorithm.

Chapter 5: Controller Implantation and Hardware

This chapter describes the hardware structure of the proposed pipe inspection robot to implement the proposed controllers, the electrical design and software developed in this thesis. All electric hardware used in the system are described such as steering motors and driving motors, encoders, industrial PC, batteries, microcontrollers, ATmega128, ultrasonic sensor, ATmega8, monitor and motor driver.

Chapter 6: Simulation and Experimental Results

This chapter presents simulation result and experiment results for the developed PIR to adjust its diameter to give reference diameters and to drive in various pipelines such as elbows, straight pipeline to show the effectiveness and the applicability of the proposed driving algorithm and the proposed controllers in chapter 4. Images are obtained through the camera sensor during the driving experiment.

Chapter 7: Conclusions and Future Works

Conclusions of this thesis and several suggestions for future works are presented.



Chapter 2. System Description and Modeling

This chapter structure describes of a pipe inspection robot (PIR) and its following modelings the dynamic modeling and expansion DC motor. Firstly, kinematic modeling of 4-bar linkage of the proposed pipe inspection robot is proposed to adjust the diameter of the robot. Secondly, kinematic modeling of the purposed pipe inspection robot and dynamic modelings of dynamic the driving wheel dc motor to track a reference velocity are presented.

2.1. System description

Design of a wheel type pipe inspection robot used for this thesis is shown in Fig. 2.1. The designed robot consists of active module, passive modules and universal joint. The active module uses the use DC motor to expand and contract the wheels, whereas the passive module uses the use of spring. The active module is used for giving pressure to the wall so that the robot can grip the pipe wall especially moving in elbows or vertical pipe. On the other hand, the passive module is used to support the active module in case that the active module can't move in some conditions such as moving through elbow, and/or passing through a choked section in pipeline. The universal joint is used to connect the active module and the passive module together and give more flexibility with any direction when the robot moving inside pipeline.

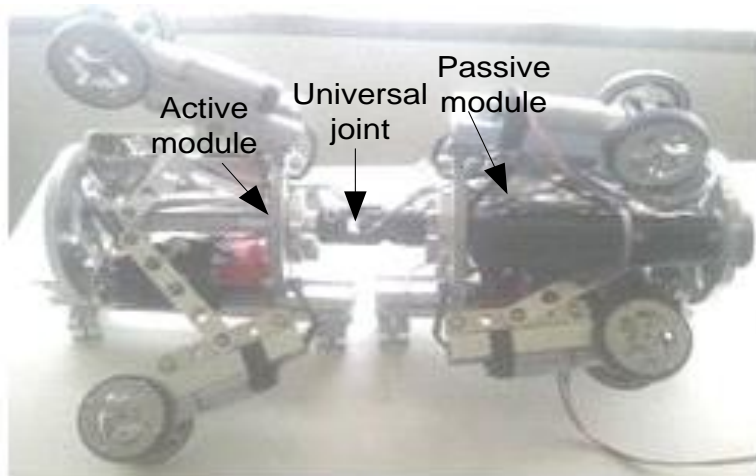


Fig. 2.1 Design of a wheeled type pipe inspection robot used for this thesis

Fig. 2.2 shows the structure of the active module. This module consists of three wheel configurations, a thread shaft, three 4-bar linkages, two gears and a high power 33.5W expansion motor to expand and contract the wheels. Each wheel configuration consists of a 12.8W DC motor for driving motor and rubber double type wheel sets. 4-bar linkages are used to assure the robot to have strong grip on the pipe wall as depicted in Fig. 2.3. Rubber wheels make the wheel give bigger wall press forces. Expansion and contraction of the 4-bar linkage is done by rotating the thread shaft which is actuated by expansion motor and thus making the shaft holder move forward and backward. Shaft holder in Fig. 2.3 is used to transfer energy from thread shaft to the 4-bar linkage.

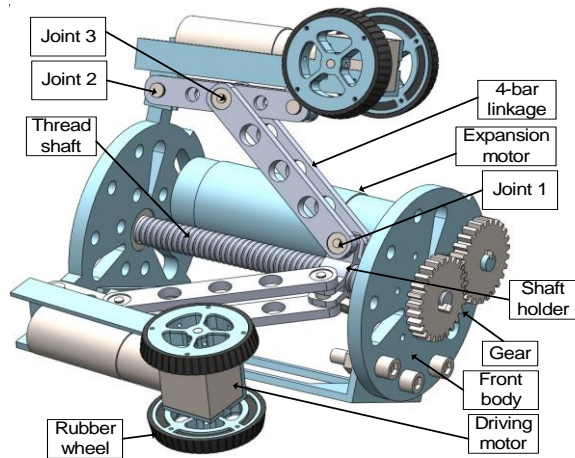


Fig. 2.2 Structure of the active module

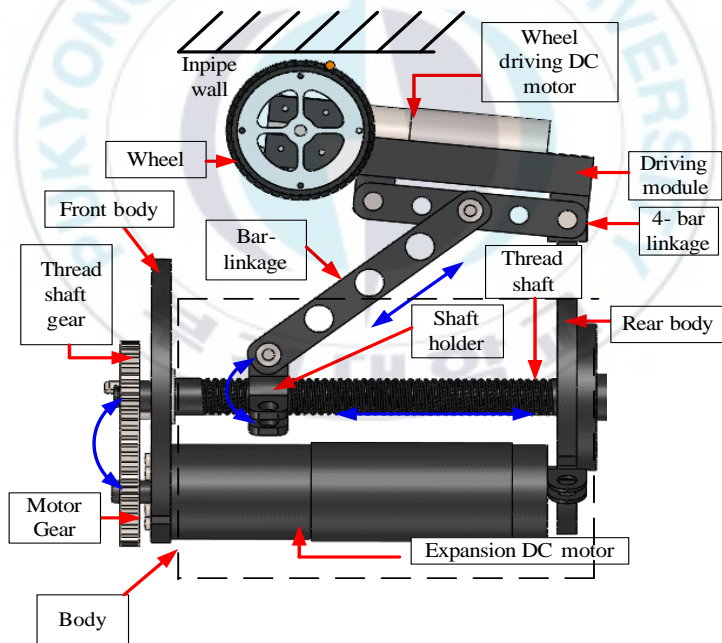


Fig. 2.3 Side view of the active module

Fig. 2.4 depicts the structure of the passive module. Passive module has similar structure with the active module. Instead of thread shaft in the active module, compression spring is used for expansion and contraction of 4-bar linkage in the passive module. This is because the proposed pipe inspection robot only needs one active module to work in pipelines.

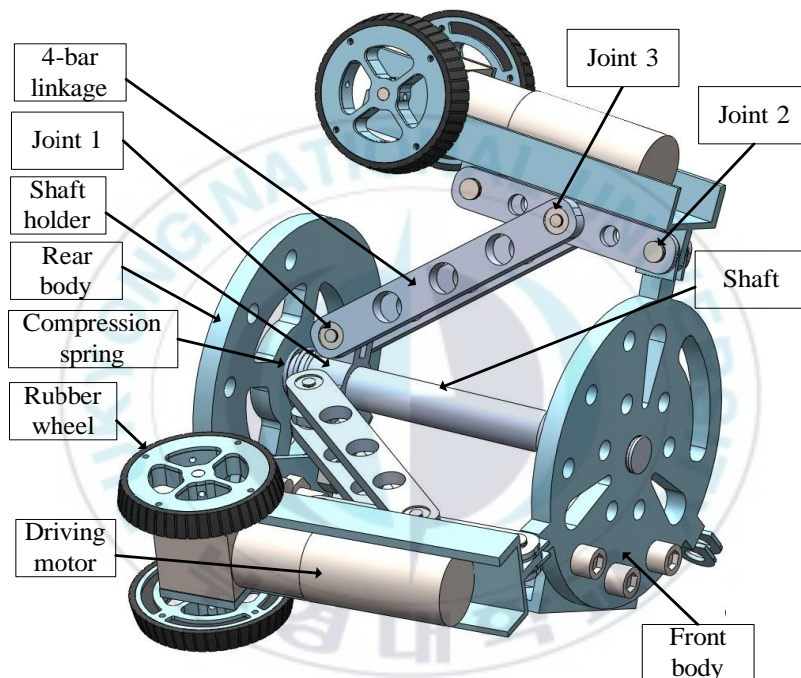


Fig. 2.4 Structure of the passive module

Fig. 2.5 shows the universal joint of PIR which connects together with the active module and the passive module to give flexible movement in all directions.

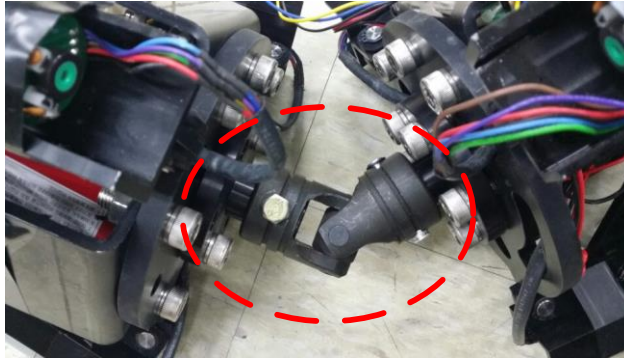


Fig. 2.5 Universal joint

Fig. 2.6 shows a driving module of the proposed pipe inspection robot connected with the 4-bar linkage and it consists of a wheel driving motor and motor case and doubled driving type wheel three pair driving modules in the active module and passive module are respectively. The active modules and the passive module are installed in the proposed pipe inspection robot.

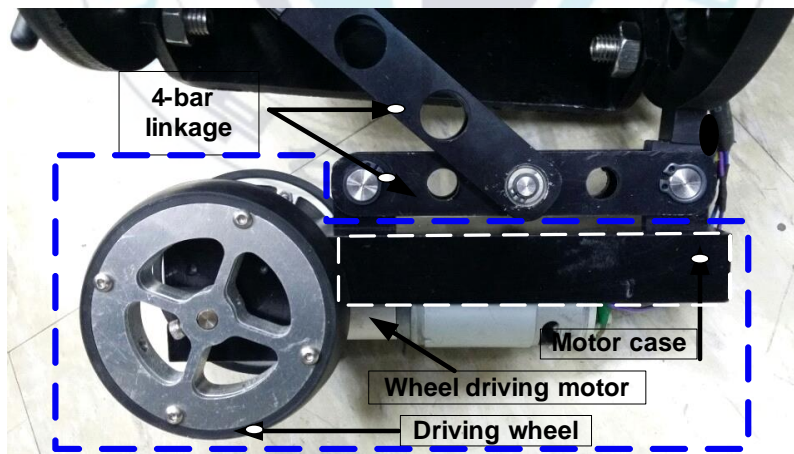


Fig. 2.6 Structure of the driving module

The specification of the pipe inspection robot is shown in Table 2.1

Table 2.1 Specification of the pipe inspection robot used for this thesis

Specification	Value(Unit)	Specification	Value(Unit)
Total weight	11 kg	Total length of the robot	685 mm
Length of active module	255 mm	Exterior diameter	300-500 mm
Weight of active module	5.5 kg	Nominal speed	9 cm/s
Length of passive module	220 mm	Maximum speed	21 cm/s
Weight of passive module	4.5 kg	Camera module length	135 mm
Gear ratio	1:1		

2.2. System modeling

2.2.1. Diameter adjusting modeling

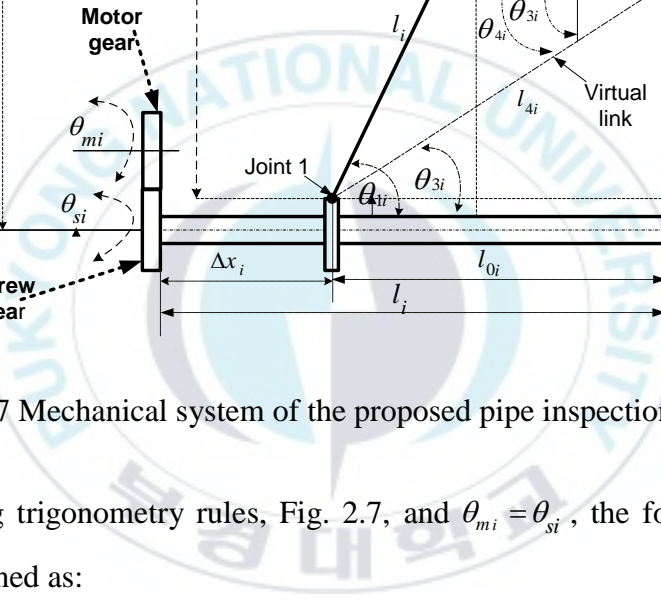
In this section, firstly, kinematic modeling of 4-bar linkage of the pipe inspection robot is used to adjust the diameter of the pipe inspection robot. Secondly, dynamic modeling of expansion dc motor to adjust the 4-bar linkage of the active module is introduced. The nomenclatures of symbols used in the modeling are shown in Table 2.2.

Table 2.2 Nomenclature of linkage and expansion DC motor

Symbol	Parameters
h_i	Distance from the center of the wheel to joint 1 of the i^{th} 4-bar linkage
θ_{1i}	Angle between link 1 and thread shaft of the i^{th} 4-bar linkage
θ_{2i}	Angle between link 2 and thread shaft of the i^{th} 4-bar linkage
θ_{3i}	Angle between virtual link and thread shaft of the i^{th} 4-bar linkage
θ_{4i}	Angle between link 3 and virtual link of the i^{th} 4-bar-linkage
θ_{5i}	Outside angle between link 2 and link 3 of the i^{th} 4-bar linkage
h_{ti}	Distance from thread shaft to wall of the i^{th} 4-bar linkage

d_{1i}	Radius from joint 1 to the center of thread shaft of the i^{th} 4-bar linkage
d_{2i}	Radius from joint 2 to the center of thread shaft of the i^{th} 4-bar linkage
Δx_i	Moving displacement of shaft holder of the i^{th} 4-bar linkage
l_{0i}	Distance between front body to shaft holder of the i^{th} 4-bar linkage
l_{1i}	Length of link 1 of the i^{th} 4-linkage the i^{th} 4-bar linkage
l_{2i}	Length of link 2 of the i^{th} 4-linkage the i^{th} 4-bar linkage
l_{3i}	Length of link 3 of the i^{th} 4-linkage of the i^{th} 4-bar linkage
l_{4i}	Length of virtual link from joint 1 to joint 2 of the i^{th} 4-bar linkage
l_i	Distance from the rear body to the front body of the i^{th} 4-bar linkage
θ_{mi}	Rotation angle of expansion DC motor of the i^{th} 4-bar linkage
r_{wi}	Radius of a driving wheel of the i^{th} 4-bar linkage
p_i	Lead of thread shaft of the i^{th} 4-bar linkage
J_i	Moment of inertia of the i^{th} 4-bar linkage
$K_{\phi i}$	Emf constant of the i^{th} 4-bar linkage
L_i	DC motor inductanc of the i^{th} 4-bar linkage
u_i	DC motor voltage of the i^{th} 4-bar linkage
b_i	Viscous friction of the i^{th} 4-bar linkage
R_i	DC motor resistance of the i^{th} 4-bar linkage
i_{mi}	DC motor current of the i^{th} 4-bar linkage
s_i	Rotantioal angale of thred shaft of the i^{th} 4-bar linkage

The mechanism system of the active module in Fig. 2.7 is shown in Fig. 2.7.



Using trigonometry rules, Fig. 2.7, and $\theta_{mi} = \theta_{si}$, the followings are obtained as:

$$\Delta x_i = \frac{p}{2\pi} \theta_{mi} \quad (2.1)$$

$$l_{0i} = l_i - \Delta x_i \quad (2.2)$$

$$l_{4i} = \sqrt{l_{0i}^2 + (d_{2i} - d_{1i})^2} \quad (2.3)$$

$$\theta_{3i} = \tan^{-1} \left(\frac{d_{2i} - d_{1i}}{l_{0i}} \right) = \sin^{-1} \left(\frac{d_{2i} - d_{1i}}{l_{4i}} \right) = \cos^{-1} \left(\frac{l_{0i}}{l_{4i}} \right) \quad (2.4)$$

$$\theta_{4i} = \cos^{-1} \left(\frac{l_{2i}^2 + l_{4i}^2 - l_{1i}^2}{2l_{2i}l_{4i}} \right) \quad (2.5)$$

$$\theta_{2i} = \theta_{4i} - \theta_{3i} \quad (2.6)$$

$$h_{ti} = d_{2i} + l_{2i} \sin \theta_{2i} + l_{3i} \sin(\theta_{5i} - \theta_{2i}) + r_{wi} \quad (2.7)$$

The moving displacement of shaft holder Δx_i of the i^{th} linkage is controlled by changing the rotation angle of explanation DC motor. The expansion DC motor system is shown in Fig. 2.8.

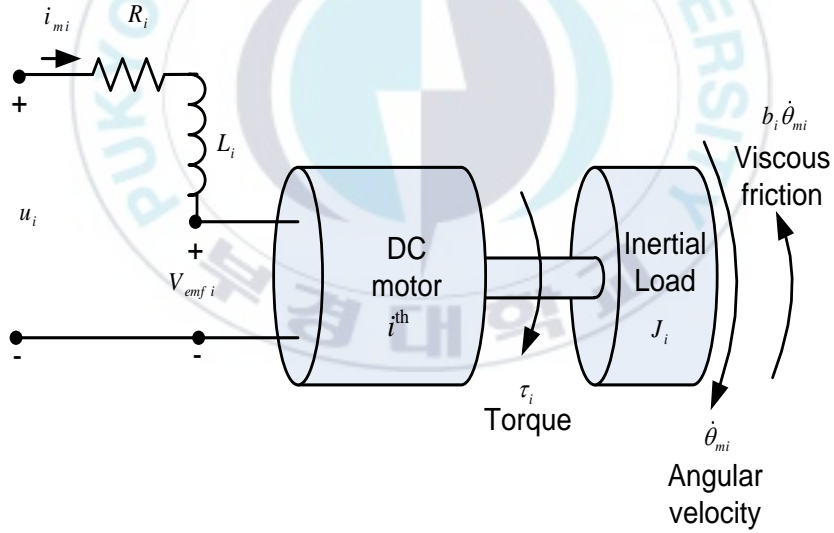


Fig. 2.8 DC expansion motor system

The system equation of the DC expansion motor is expressed by

$$\dot{\mathbf{x}}_i = \mathbf{A}_i \mathbf{x}_i + \mathbf{B}_i u \quad (2.8)$$

$$\mathbf{A}_i = \begin{bmatrix} -\frac{R_i}{L_i} & -\frac{K_{\phi i}}{L} \\ \frac{K_{\phi i}}{J_i} & -\frac{b_i}{J_i} \end{bmatrix}, \mathbf{B}_i = \begin{bmatrix} \frac{1}{L_i} \\ 0 \end{bmatrix}, \mathbf{x}_{i_i} = \begin{bmatrix} i_{m_i} & \dot{\theta}_{m_i} \end{bmatrix}^T$$

where \mathbf{x}_i is the i^{th} system state variable vector, u_i is the i^{th} motor voltage as an control input, and the rotational angle of the i^{th} expansion DC motor can be obtained as follows:

$$\theta_{m_i} = \int \dot{\theta}_{m_i} dt + \theta_{m_i}(0) \quad (2.9)$$

The tracking error of radius for the pipe inspection robot is defined as follows:

$$e_{hi} = h_{ref_i} - h_{t_i} \quad (2.10)$$

where h_{ref_i} is reference radius of the pipe inspection robot.

2.2.2. Driving speed modeling

Kinematic modeling is used to design a controller for the proposed PIR to track a reference angular velocity. Fig. 2.9 shows coordinate frames for the PIR kinematic modeling.

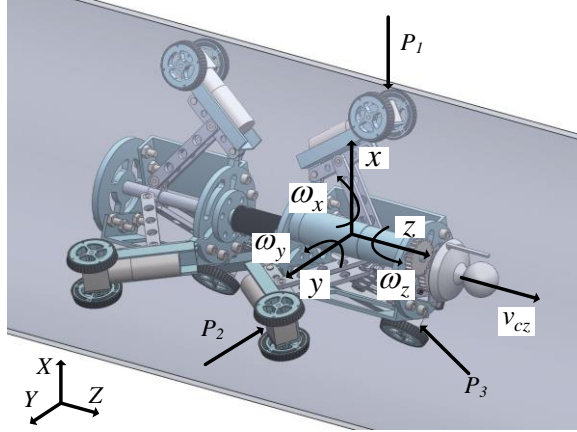


Fig. 2.9 Coordinate frame of the proposed pipe inspection robot

XYZ denotes the global coordinate frame, whereas represents the local coordinate frame at the geometric center of the PIR \hat{i} , \hat{j} , and \hat{k} are the unit vectors of the local coordinate frame. The axis is always in parallel with P_i regardless of how the PIR moves, where P_i (for $i = 1$ to 3) is normal forces of the pipe wall to the wheels with respect to axes.

By assuming that linear velocities of all wheels v_1 , v_2 and v_3 exist, the total angular velocity vector of the PIR is

$$\omega = \omega_x \hat{i} + \omega_y \hat{j} \quad (2.11)$$

$$\omega_x = \frac{\sqrt{3}r_w}{3h_t} \dot{\theta}_2 - \frac{\sqrt{3}r_w}{3h_t} \dot{\theta}_3 \quad (2.12)$$

$$\omega_y = -\frac{2r_w}{3h_t} \dot{\theta}_1 + \frac{r_w}{3h_t} \dot{\theta}_2 + \frac{r_w}{3h_t} \dot{\theta}_3 \quad (2.13)$$

where ω_x, ω_y are angular velocities about x, y axes, respectively. $\dot{\theta}_1$, $\dot{\theta}_2$ and $\dot{\theta}_3$ are input angular velocities of the three wheels. r_w is

radius of the wheels and h_t is the distance from the center of the pipe inspection robot to the center of the wheel.

The linear velocity at the center of the pipe inspection robot is obtained by taking the average of linear velocities of the wheel as follows:

$$v_{cz} = \frac{1}{3}(v_1 + v_2 + v_3) = \frac{r_w}{3}(\dot{\theta}_1 + \dot{\theta}_2 + \dot{\theta}_3) \quad (2.14)$$

The relationship between the input angular velocity vector of wheels $\dot{\theta}_a = [\dot{\theta}_1 \ \dot{\theta}_2 \ \dot{\theta}_3]^T$ and the output velocity vector of the PIR is given as $\eta = [\omega_x \ \omega_y \ v_{cz}]^T$ is given as follows:

$$\eta = [G_a^u] \dot{\theta}_a \quad (2.15)$$

and the following Jacobean is given in case that h_t is constant.

$$[G_a^\eta] = \frac{\partial \eta}{\partial \dot{\theta}_a} = \begin{bmatrix} 0 & \frac{\sqrt{3}r_w}{3h_t} & -\frac{\sqrt{3}r_w}{3h_t} \\ -\frac{2r_w}{3h_t} & \frac{r_w}{3h_t} & \frac{r_w}{3h_t} \\ \frac{r_w}{3} & \frac{r_w}{3} & \frac{r_w}{3} \end{bmatrix} \quad (2.16)$$

The tracking velocity error vector of the pipe inspection robot is defined as follows:

$$\mathbf{e} = \begin{bmatrix} e_1 \\ e_2 \\ e_3 \end{bmatrix} = \begin{bmatrix} \omega_{rx} \\ \omega_{ry} \\ v_{rcz} \end{bmatrix} - \begin{bmatrix} \omega_x \\ \omega_y \\ v_{cz} \end{bmatrix} = \boldsymbol{\eta}_r - \boldsymbol{\eta} \quad (2.17)$$

where $\boldsymbol{\eta}_r = [\omega_{rx} \ \omega_{ry} \ v_{rcz}]^T$ is the reference is the reference velocity vector of the PIR.

The tracking angular velocity error vector of the wheels is defined as:

$$\mathbf{e}_\theta = \begin{bmatrix} e_{\theta 1} \\ e_{\theta 2} \\ e_{\theta 3} \end{bmatrix} = \begin{bmatrix} \dot{\theta}_{1r} \\ \dot{\theta}_{2r} \\ \dot{\theta}_{3r} \end{bmatrix} - \begin{bmatrix} \dot{\theta}_1 \\ \dot{\theta}_2 \\ \dot{\theta}_3 \end{bmatrix} = \dot{\boldsymbol{\theta}}_{ar} - \dot{\boldsymbol{\theta}}_a \quad (2.18)$$

where $\dot{\boldsymbol{\theta}}_{ar}$ is the reference input angular velocity vector of wheels.

The relation between \mathbf{e}_θ and \mathbf{e} is given by

$$\mathbf{e}_\theta = (\mathbf{G}_a^u)^{-1} \mathbf{e} \quad (2.19)$$

The DC expansion motor system of the i^{th} 4-bar linkage is shown in Fig. 2.6. The differential equation describing the dynamics of the i^{th} DC motor system is expressed a state space model as follows:

$$\dot{\mathbf{x}}_i = \mathbf{A}_i \mathbf{x}_i + \mathbf{B}_i u_i \quad (2.20)$$

$$\mathbf{A}_i = \begin{bmatrix} -\frac{R_i}{L_i} & -\frac{K_{\phi i}}{L_i} \\ \frac{K_{\phi i}}{J_i} & -\frac{b_i}{J_i} \end{bmatrix}, \mathbf{B}_i = \begin{bmatrix} \frac{1}{L_i} \\ 0 \end{bmatrix}, \mathbf{x}_i = \begin{bmatrix} i_{mi} & \dot{\theta}_{mi} \end{bmatrix}^T \quad (2.21)$$

where both the state variable vector of the i^{th} driving DC motor system $\mathbf{x}_i = \begin{bmatrix} i_i & \dot{\theta}_i \end{bmatrix}^T$ and measurement variable vector of the i^{th} driving DC motor system constant of motor current of the i^{th} DC motor system and the i^{th} wheel angular velocity, and $\dot{\theta}_{mi}$. The i^{th} system input vector $\mathbf{u}_i(t) = v_{mi}$ is the i^{th} motor voltage, and $\mathbf{i}_m = \begin{bmatrix} i_{m1} & i_{m2} & i_{m3} \end{bmatrix}^T$ is the current vector of the i^{th} driving DC motor ($i=1,2,3$).

Chapter 3. Driving Algorithm

When the proposed in-pipe inspection robot moves in curve pipeline, each wheel has to operate differentially to prevent the wheel from slip and overload. From this reason, a method of driving in curve pipeline is needed.

3.1. Curved pipe

In this section, a method of moving the robot in the curve pipeline is presented in Fig. 3.1. In curved pipelines, the wheel velocities need to be different depending on the contact position of with the wall because three wheels have different travelling distances in S of start and finish of curved.

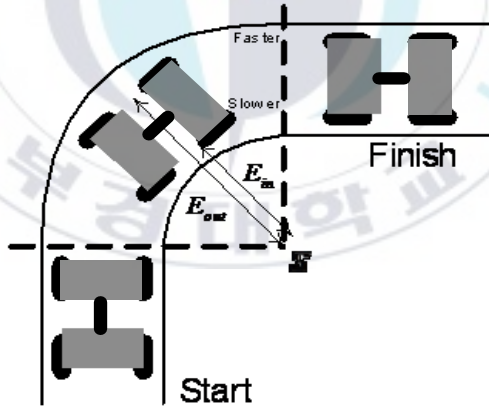


Fig. 3.1 Driving principle of in-pipe inspection robot

Fig. 3.2 presents distances between axis of center of curvature of inner pipeline contact points (1, 2, 3) of three wheels and each wheel. Distances from center axis of curvature to each wheel are presented as R_p , R_q , R_r , and their ratio is same with ratio of each wheel, so an

algorithm for getting ratio of curvature is needed. This is verified by infrared sensor attached on the in-pipe inspection robot.

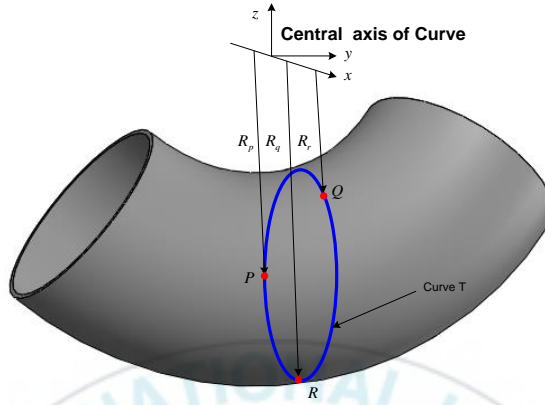


Fig. 3.2 Position of wheels in curved PIR

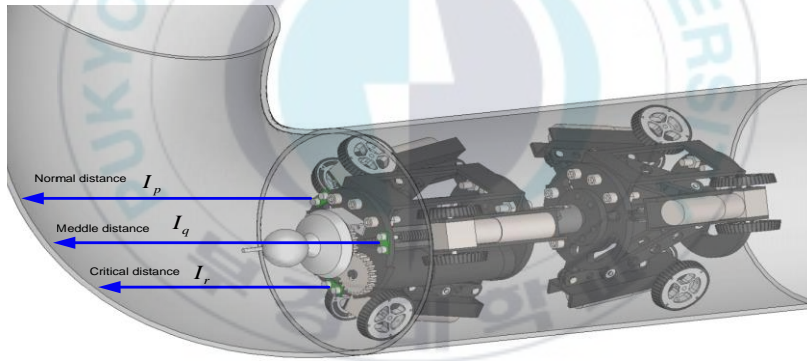


Fig. 3.3 Distance between sensor and pipeline

I_p , I_q , I_r are measured when the proposed PIR arrives at critical value, which is arbitrary distance between the inner wall of pipeline and ultrasonic sensor. The distance values are as follows:

$$\begin{cases} I_p = k_1 \times \sin \varphi + k_2 \\ I_q = k_1 \times \sin(\varphi + \frac{2}{3}\pi) + k_2 \\ I_r = k_1 \times \sin(\varphi + \frac{4}{3}\pi) + k_2 \end{cases} \quad (3.1)$$

where k_1, k_2 are decided by size of elbow's radius are constant values and they can be obtained by simulation.

Ratio of curvature radii R_p, R_q, R_r can be gotten through I_p, I_q, I_r moving although phase difference between R_p, R_q, R_r and I_p, I_q, I_r is about $-\pi$ radian.

Relation between ω_i and R_i is shown in Fig. 3.4. The relation between the wheel angular velocities and the wheel linear velocities can be expressed as follows:

$$\begin{cases} v_{1ref} = V_p = R_p \omega_c = r_w \omega_{w1ref} \\ v_{2ref} = V_q = R_q \omega_c = r_w \omega_{w2ref} \\ v_{3ref} = V_r = R_r \omega_c = r_w \omega_{w3ref} \end{cases} \quad (3.2)$$

where $v_{iref} (i=1, 2, 3)$ is reference wheel linear velocity of each wheel, R_i is distance from the center axis of curvature to each wheel, ω_c is the angular velocity of the center of curvature, and r_w is radius of the wheel. From Eq. (3.2), the reference angular velocities of the i^{th} wheel $\omega_{wiref} (i=1, 2, 3)$ are calculated as:

$$\begin{aligned}
\omega_{w1ref} &= \omega_p = \dot{\theta}_{1ref} = \frac{V_p}{r_w} \\
\omega_{w2ref} &= \omega_q = \dot{\theta}_{2ref} = \frac{V_q}{r_w} \\
\omega_{w3ref} &= \omega_r = \dot{\theta}_{3ref} = \frac{V_r}{r_w}
\end{aligned} \tag{3.3}$$

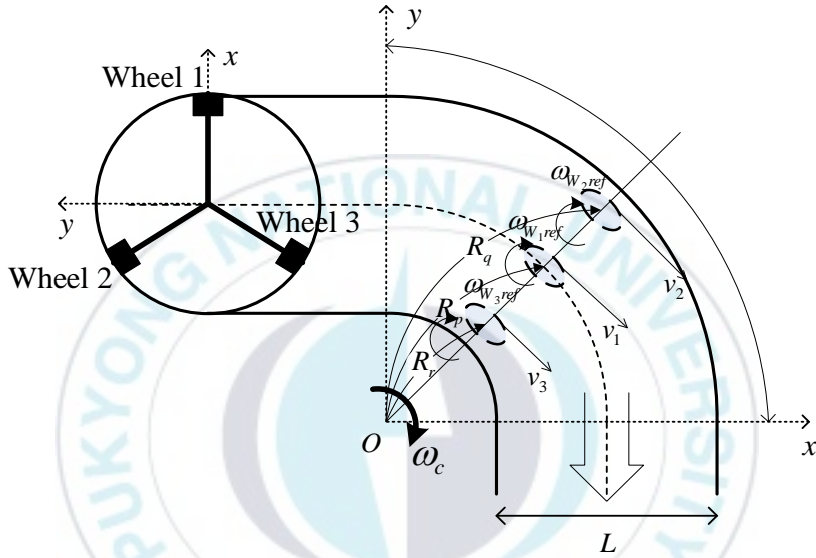


Fig. 3.4 Relation between ω_{wiref} and R_i

3.2. Simulation results in curved pipe

The location of points P,Q , R of the proposed PIR in the curved pipeline is shown in Fig. 3.5 and ϕ is rotation angle of the proposed PIR.

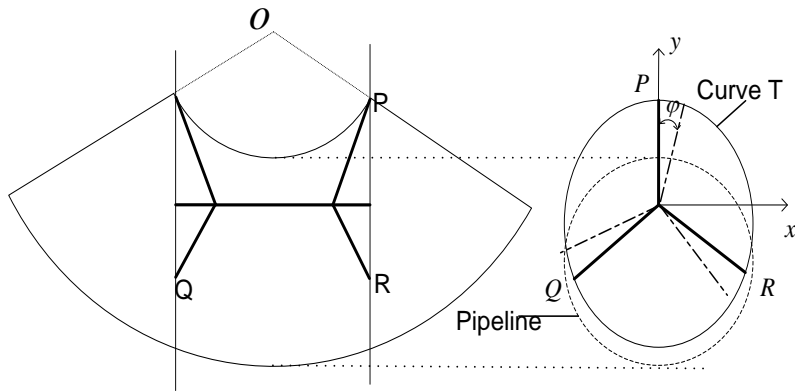


Fig. 3.5 In-pipe inspection robot in curved pipe

Fig. 3.6 and Fig. 3.7 show the simulation results two diameter with respect to I_p , I_q , I_r of the proposed pipe inspection robot in pipeline with diameter 300 mm and 500 mm where k_1 , k_2 are each 65.245mm, 326.995mm and 81.156mm, 657.267mm obtained by the simulation, respectively.

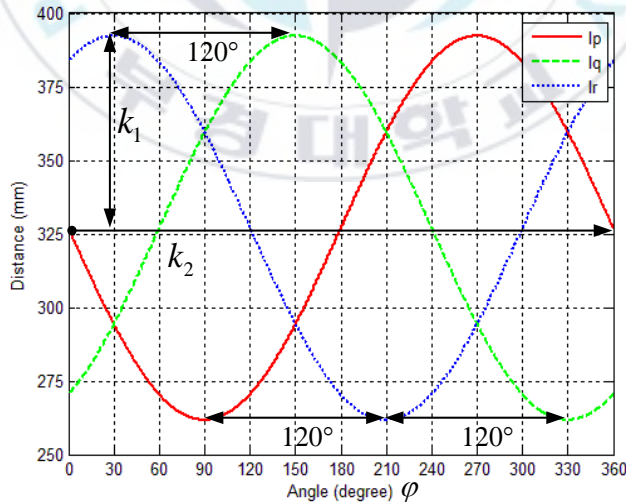


Fig. 3.6 Values of I_p , I_q , I_r in $\phi 300$ mm

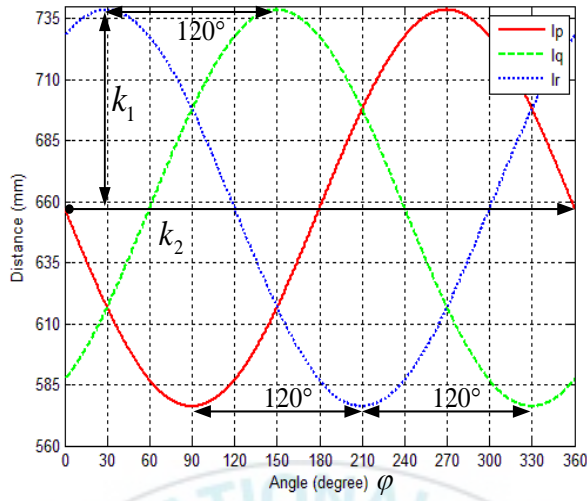


Fig. 3.7 Values of I_p , I_q , I_r in $\phi 500$ mm

These values are making a sinusoidal signal having a phase difference as much as it can be seen.

Fig. 3.8 and Fig 3.9 shows simulation results with respect to R_p , R_q , R_r of pipe the proposed inspection robot with different diameter 300mm and 500 mm, respectively.

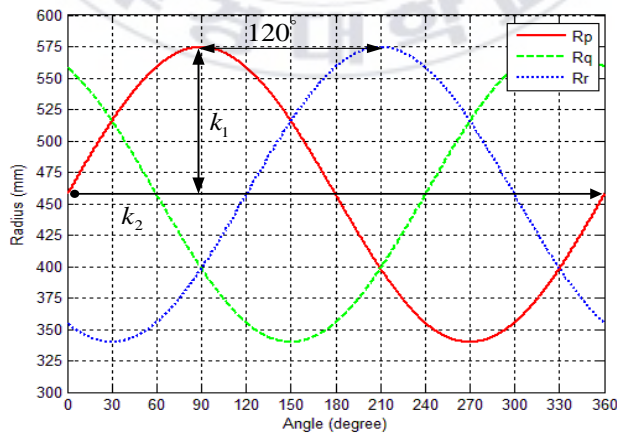


Fig. 3.8 Values of R_p , R_q , R_r in $\phi 300$ mm

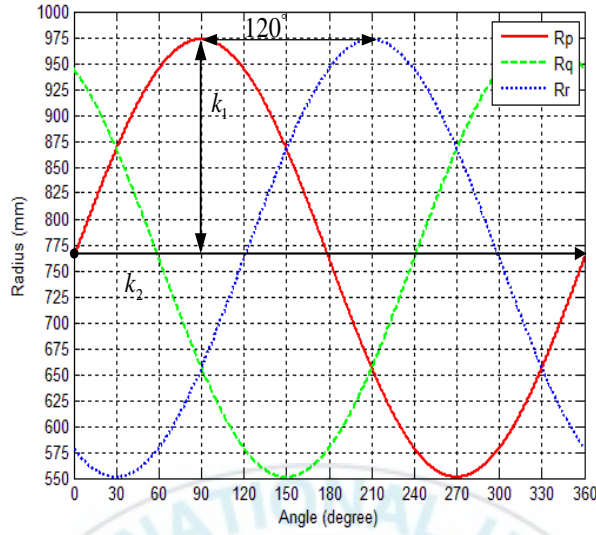


Fig. 3.9 Values of R_p , R_q , R_r in $\phi 500$ mm

The figure above also three curves in sinusoidal signal a pattern so that it is possible to ensure that with sufficient retardation. Fig. 3.8 (I_p , R_p) and Fig. 3.9 (I_q , R_q) has a phase difference of about $-\pi$ radian one another.

Fig. 3.8 and Fig. 3.9 show the linear velocities with respect I_p , I_q , I_r and the wheel angular velocities of the curvature with respect to ω_p , ω_q , ω_r corresponding to the each position of the wheels at the time of curve driving in $\phi 300$ mm and $\phi 500$ mm pipeline respectively.

Fig. 3.10, Fig. 3.11, Fig. 3.12 and Fig. 3.13 shows the linear velocities with respect I_p , I_q , I_r and the angular velocities with respect ω_p , ω_q , ω_r corresponding to the position of the wheels at the time of curve driving in $\phi 300$ mm and $\phi 500$ mm pipeline.

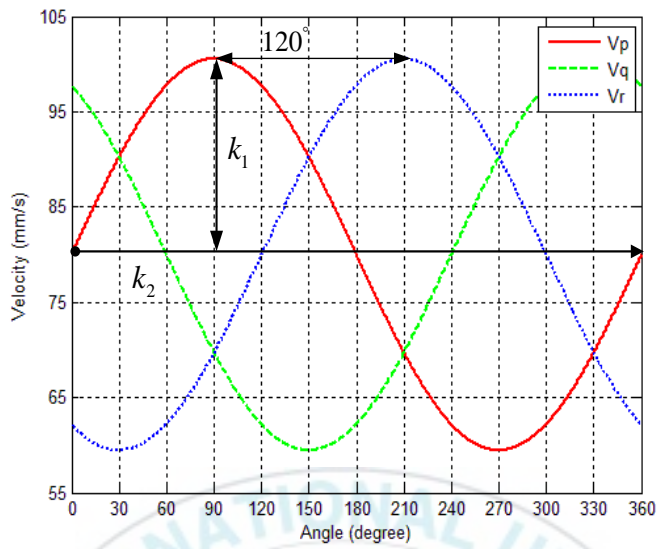


Fig. 3.10 Values of V_p , V_q , V_r in $\phi 300$ mm

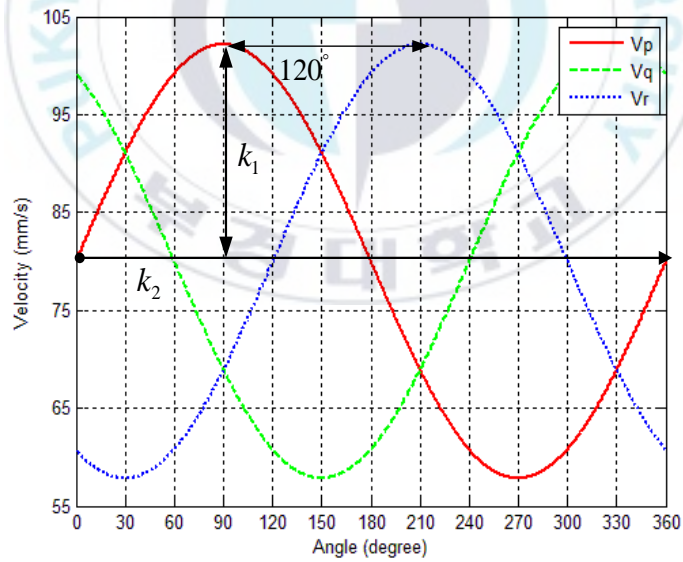


Fig. 3.11 Values of V_p , V_q , V_r in $\phi 500$ mm

Fig. 3.12 and Fig. 3.13 show ω_p , ω_q , ω_r corresponding to the value with diameter $\phi 300$ mm and $\phi 500$ mm, respectively.

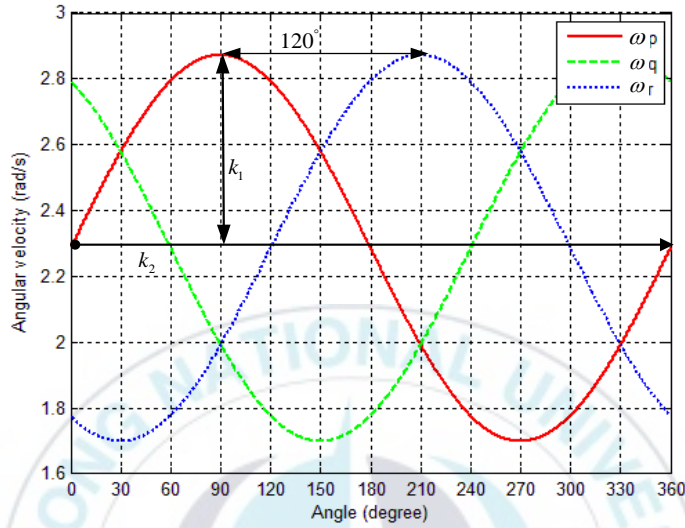


Fig. 3.12 Values of ω_p , ω_q , ω_r in $\phi 300$ mm

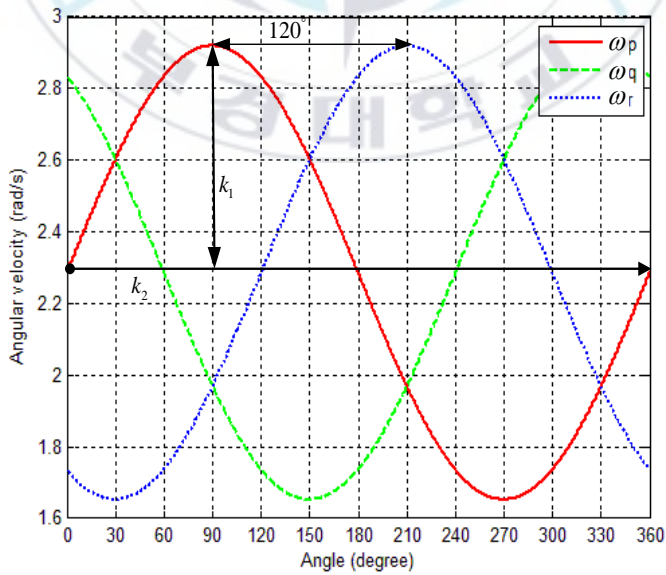


Fig. 3.13 Values of ω_p , ω_q , ω_r in $\phi 500$ mm

Fig. 3.10 shows a flow of the proposed driving algorithm for driving elbow.

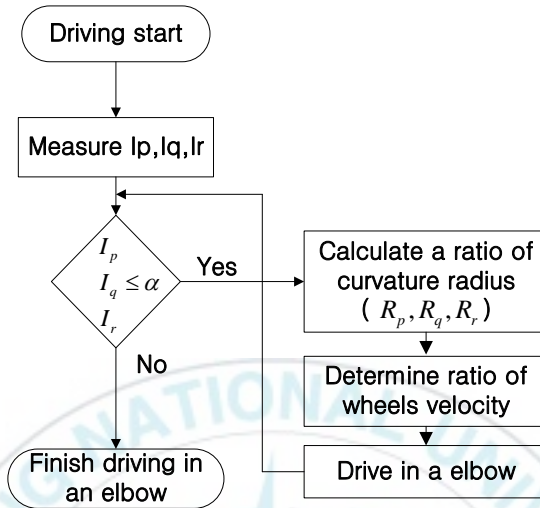


Fig. 3.14 Flow chart of the proposed driving algorithm

In Fig. 3.10, α is chosen by the simulation or experiment for the proposed pipe inspection robot.

Chapter 4. Controller Design

4.1. Diameter tracking controller design

To track given reference radii of the pipe inspection robot, a conventional PI controller and a fuzzy logic controller are proposed. The controllers are designed so that the tracking error goes to zero. The controller input u in Eq. (2.8) is defined as u_{PI} in the conventional PI controller and u_{FLC} in the fuzzy logic controller.

4.1.1. PI Controller

A conventional PI controller is used for controlling diameter of the pipe inspection robot as follows:

$$u_{PI} = K_P e_h + K_I \int e_h dt \quad (4.1)$$

where K_P and K_I are the PI controller gains.

Block diagram of the conventional PI controller is shown in Fig. 4.1.

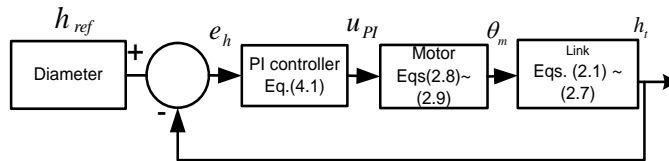


Fig. 4.1 Block diagram of the conventional PI controller

4.1.2. Fuzzy Controller

The fuzzy rules are constructed by expert experience or knowledge database. First, the tracking error e_h and the derivate of the tracking error \dot{e}_h are used as the input variables of the fuzzy logic controller. The control voltage u is chosen as the output variable of the fuzzy logic controller. The linguistic variables are defined as {NB, NS, Z, PS, PB}, where NB means negative big, NS means negative small, Z means zero, PS means positive small and PB means positive big. The input and output membership functions are shown in Figs. 4.2 ~ 4.4 as follows:

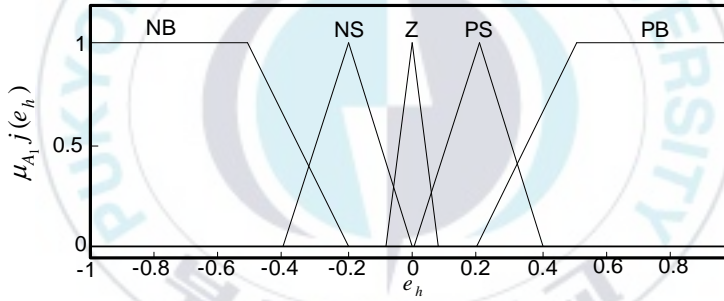


Fig. 4.2 Membership function for input e_h

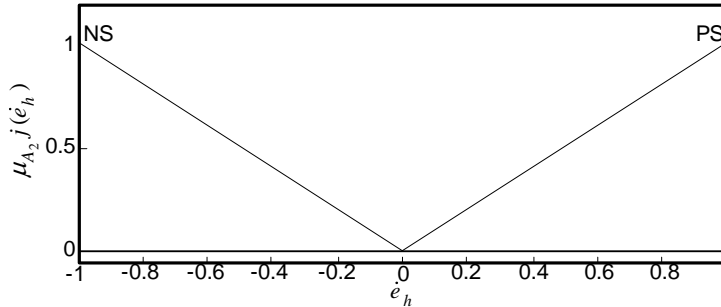


Fig. 4.3 Membership function for input \dot{e}_h

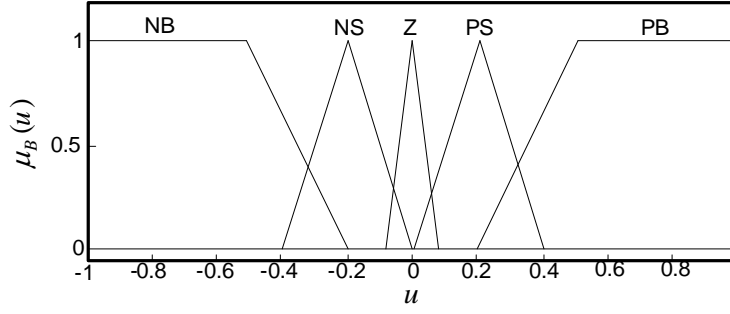


Fig. 4.4 Membership function of output u

The fuzzy rules are summarized in Table 4.1.

Table 4.1 Fuzzy rules

$\dot{e}_h \backslash e_h$	NS	PS
NB	NB	NB
NS	NS	NS
Z	NS	PS
PS	PS	PS
PB	PB	PB

The type of fuzzy inference engine used in this thesis is Mamdani's method. In this thesis, max-min type decomposition is used and the final output for system is calculated by using the center of area gravity method as follows:

$$\mu_B(u) = \max \left[\mu_{A_1} j(\mathbf{e}_\theta), \mu_{A_2} j(\dot{e}_\theta), \mu_B j(u) \right] \quad (4.2)$$

$\mu_{A_1} j(e_h)$ = the membership of e_h ,

$\mu_{A_2} j(\dot{e}_h)$ = the membership function \dot{e}_h ,

$\mu_B j(u)$ = the membership function of u ,

j an index of every membership function of fuzzy set.

Fuzzy logic output can be calculated by the center of gravity defuzzification as:

$$u_{FLC} = \frac{\sum_{i=1}^m \mu_B(u_i) \cdot u_i}{\sum_{i=1}^m \mu_B(u_i)} \quad (4.3)$$

where m is the number of rules and is the inference result.

Block diagram of the proposed fuzzy logic controller is shown in Fig. 4.5.

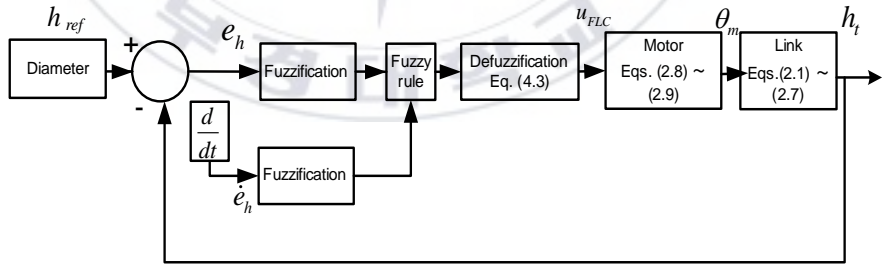


Fig. 4.5 Block diagram of the proposed fuzzy logic controller for this thesis

4.2. Driving Controller

To control wheel angular velocities of the proposed pipe inspection, a conventional PI controller and a fuzzy logic controllers are proposed as follows:

4.2.1. PI Controller

A conventional PI controller is used for controlling wheel reference velocity of each wheel of the pipe inspection robot as follows:

$$u_{PI} = K_p e_\theta + K_I \int e_\theta dt \quad (4.4)$$

where K_p and K_I are the PI controller gains.

Block diagram of the conventional PI controller is shown in Fig. 4.6

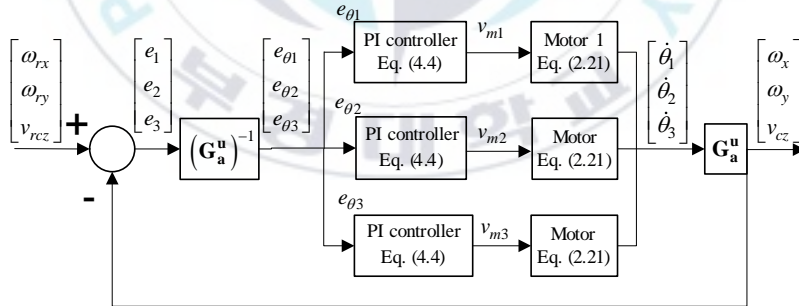


Fig. 4.6 Block diagram of the conventional PI controller

4.2.2. Fuzzy Controller

The fuzzy rules are constructed by expert experience or knowledge database. First, the i^{th} tracking wheel angular velocity

e_{θ_i} and its i^{th} derivative \dot{e}_{θ_i} are used as the input variables of the fuzzy logic controller. The i^{th} control law as supplied voltage u_{di} for motor drive is chosen as the i^{th} output variable of the fuzzy logic controller. The linguistic variables are defined as {NB, NS, Z, PS, PB}, where NB means negative big, NS means negative small, Z means zero, PS means positive small and PB means positive big. The input and output membership functions for diving proposed pipe inspection robot are shown in graphics follows:

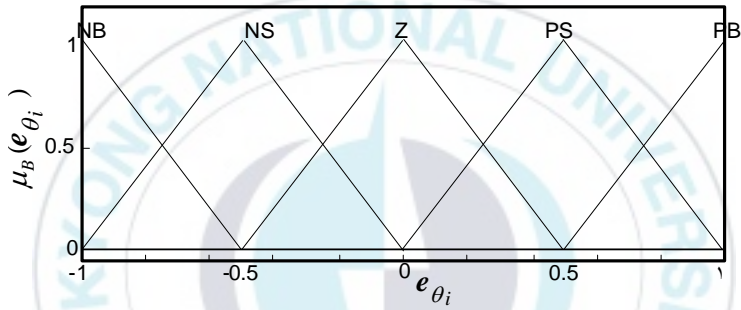


Fig. 4.7 Membership function for input e_{θ_i}

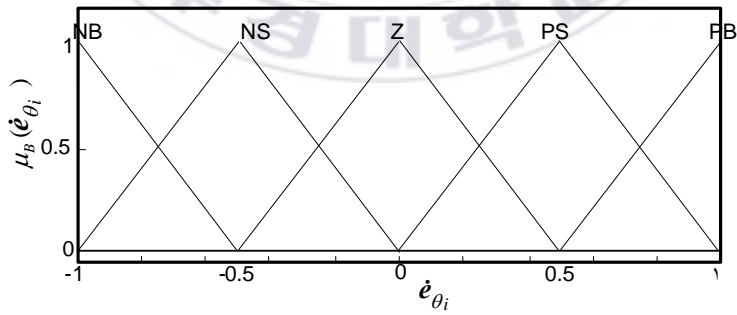


Fig. 4.8 Membership function for input \dot{e}_{θ_i}

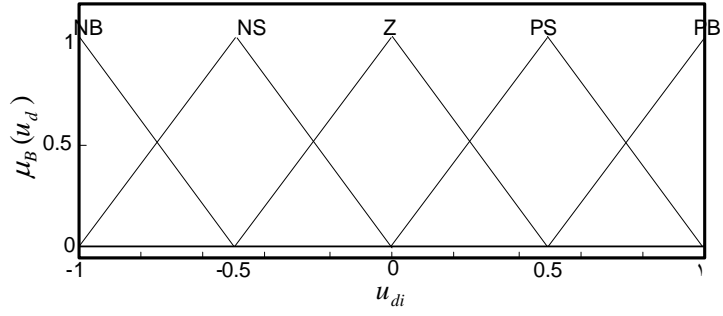


Fig. 4.9 Membership function of output u_{di}

The fuzzy rules are summarized in Table 4.2.

Table 4.2 Fuzzy rules

$\dot{e}_{\theta_i} \backslash e_{\theta_i}$	NS	PS
NB	NB	NB
NS	NS	NS
Z	NS	PS
PS	PS	PS
PB	PB	PB

The type of fuzzy inference engine used in this thesis is Mamdani's method. In this thesis, max-min type decomposition is used and the final output for system is calculated by using the center of area gravity method as follows:

$$\mu_B(u_{di}) = \max[\mu_{A_1}j(e_{\theta_0}), \mu_{A_2}j(\dot{e}_{\theta}), \mu_B j(u_{di})] \quad (4.5)$$

where

$\mu_{A_i}j(e_{\theta_i})$ = the membership of e_{θ} of i^{th} motor,

$\mu_{A_2}^j(\dot{e}_{\theta_i})$ = the membership function \dot{e}_{θ_i} of i^{th} motor,

$\mu_B^j(u_{di})$ = the membership function of u_{di} of i^{th} motor,

u_{di} = is motor voltage supplied for motor drive,

j an index of every membership function of fuzzy set.

Fuzzy logic output can be calculated by the center of gravity defuzzification as:

$$u_{FLC} = \frac{\sum_{i=1}^m \mu_B(u_{di}) \cdot u_{di}}{\sum_{i=1}^m \mu_B(u_{di})} \quad (4.6)$$

where m is the number of rules and is the inference result.

Block diagram of the proposed fuzzy logic controller is shown in Fig. 4.10.

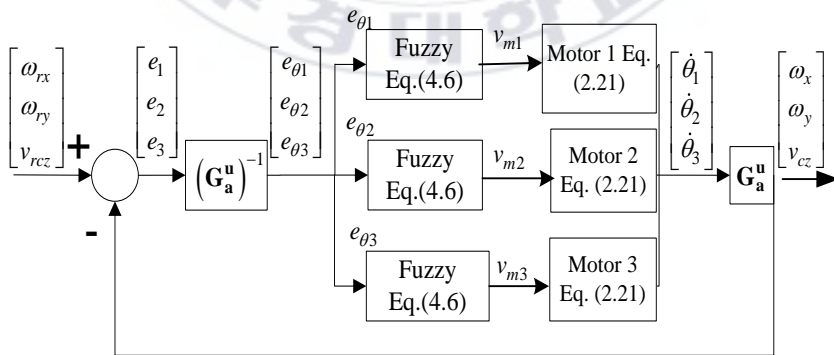


Fig. 4.10 Block diagram of the proposed fuzzy logic controller for this thesis

Chapter 5. Controller Implementation

5.1. Hardware Architecture

This chapter describes the designed and developed pipe inspection robot that consists of electrical design and software development for experimental purpose. The electrical design consists of motors, industrial PC, battery, ATmega8 microcontroller, motor driver, angular sensor and ultrasonic sensor, etc.

In the implementation, active and passive modules are connected with a universal joint to give their flexibility. Wireless camera sensor, VIJE IP-2000 PTW as shown in Fig. 5.1 is used for the developed PIR to drive smoothly inside pipeline by monitoring its movement and to get data inside pipeline. The purpose for collaboration of active and passive modules is to support each other in moving in pipelines as shown in Fig. 5.2. If the active module cannot move in a certain position, the passive module pushes/pulls the active module for the developed PIR to move. Likewise, if the passive module cannot move, the active module pulls/ pushes the passive module.



Fig. 5.1 Wireless camera VIJE IP-2000 PTW

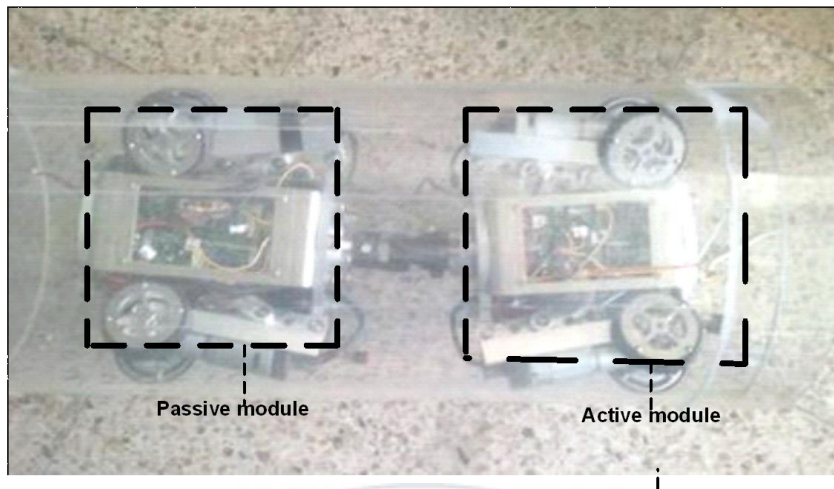


Fig. 5.2 Collaborative structure between two modules

A computer with a Graphic User Interface (GUI) is provided for users to control the developed PIR manually and obtains vision information inside the pipe. Fig. 5.3 is a flow chart of the proposed control system showing how the developed PIR works. Control commands which are given by users in GUI are sent to ATmega8. Then, ATmega8 transforms it into Pulse Width Modulation (PWM). After that, DC Motor is actuated by the PWM and finally the developed PIR is driven by the DC motor. Information data inside the pipe is obtained from two sensors, i.e. camera and encoder. The encoder converts information from one format to another, for the purposes of standardization of velocity speed, the position of the robot can be examined. ATmega128 sends signals from 3 ultrasonic sensors to computer.

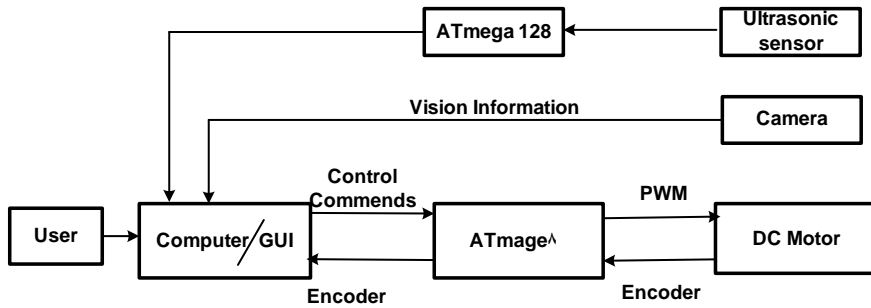


Fig. 5.3 Flow chart of the proposed control system

The control PC of the control system is used to display GUI and vision information obtained from camera. The motor control module consists of multipoint control unit (MCU), ATmega8, a motor driver and a microcontroller (AVR).

Fig. 5.4 shows the picture of the developed pipe inspection robot system.

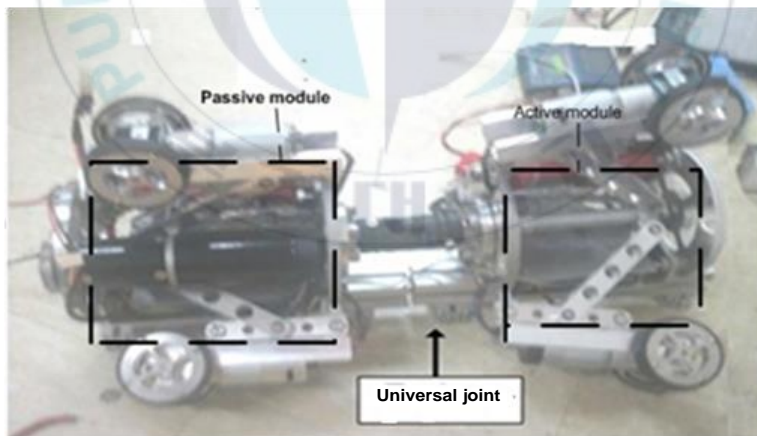


Fig. 5.4 Developed in-pipe inspection robot

5.2. Electrical part design

The electrical part design of the proposed pipe inspection robot is shown in Fig. 5.5. The electrical part design in this thesis consists of

expansion DC motor, microcontrller AVR ATmega128, ultrasonic sensor, micocontroller AVR ATmega8, motor drivers and angle sensor.

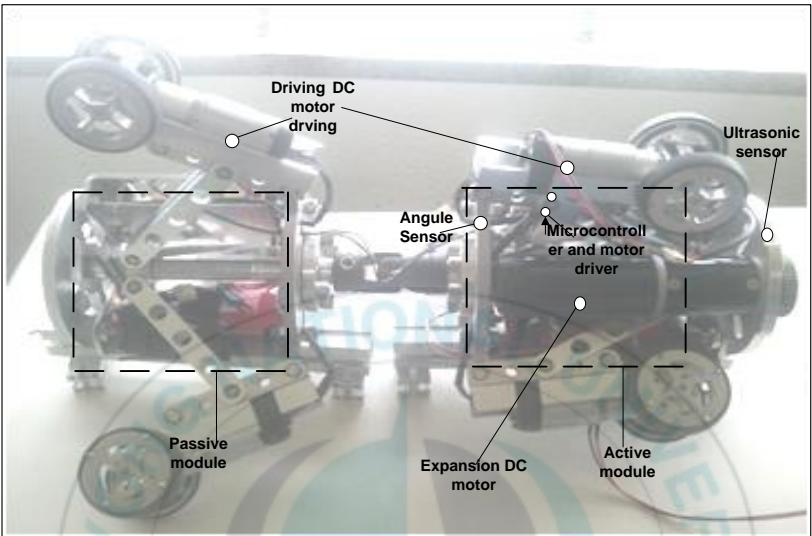


Fig. 5.5 Electrical part design of the proposed pipe inspection robot

5.2.1. Expansion DC motor

In Fig. 5.6, expansion DC motor driving the active module is shown and its specifiction is shown in the Table 5.1. It is a motor generating pressing force between driving wheels and inner wall of pipeline by controlling the rotation of the thread shaft and expanding and shrinking 4-bar linkages of active module.



Fig. 5.6 Expansion DC motor

Table 5.1 Specification of expansion DC motor IG-52 GM 03 Type

Item	Specification
Ratio	1/3 ~ 1/676 (Reduction rule 18grades)
Rated torque	3.6 kg/cm ~ 100kg/cm
Rated rotational speed	4.1 rpm ~1,000 rpm
Motor	DC 24V / 4.000rpm / 48.6 W
Encoder	38Pulses(19Pulses 2CH)

5.2.2. Microcontrollers AVR ATmega8 and ATmega128

Microcontroller AVR ATmega8 is used to convert control signals generated by the controller to PWM signals as shown in Fig. 5.7 and its specification is shown Table in 5.2.

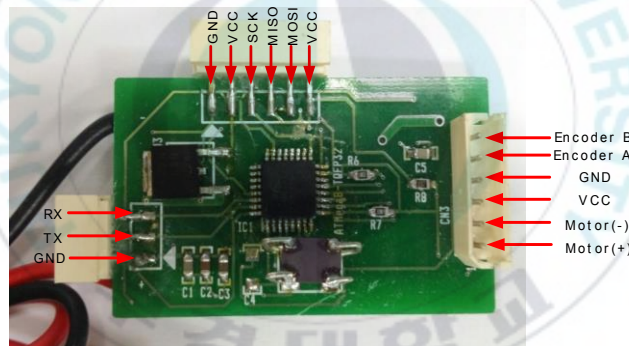


Fig. 5.7 Microcontroller Part

Table 5.2 Specification of microcontroller AVR ATmega8

Item	Specification
Operating	– 4.5V - 5.5V (ATmega8)
Speed	16MHz (ATmega8)
Power	Active: 3.6mA

Microcontrollers ATmega128 is used to receive signals from 3 ultrasonic sensors and transfer them to computer. The ATmega128 is shown in Fig. 5.8. The specification of ATmega128 is listed in Table 5.3.

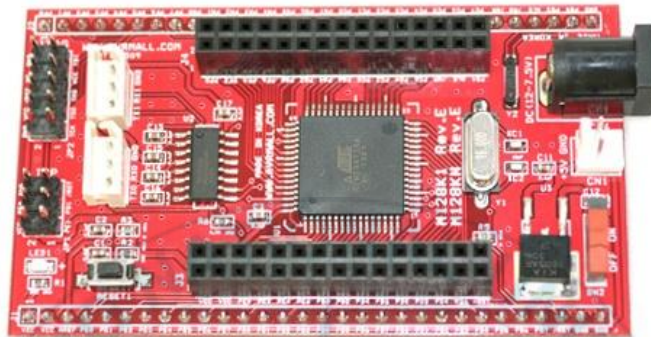


Fig. 5.8 Microcontroller AVR ATmega128

Table 5.3 Specification of microcontroller AVR ATmega128

No	Parameters	Remarks
1	Clock	16MHz
2	RS232 channel interface	Two
3	Operating power	4.5 to operate at 5.5V
4	Board size	4.6 x 7.9 cm
5	RTC-32.768KH	Available
6	ATMEL ISP port, JTAG port	Available
7	All PORT Pin Extension	Available
8	RESET switch	Available
9	Power LED (RED)	Available
10	External input power supply	Available: DC jack (power supply 7.5 ~ 12V Input)

5.2.3. Motor driver

In this thesis, the motor driver shown in Fig. 5.9 is installed with a microcontroller unit and its specifications are shown in Table 5.4. Motor drivers for 7 driving DC motors such 3 driving DC motor in passive module, 3 driving DC motors in active module and one DC motor for expansion in active are used.

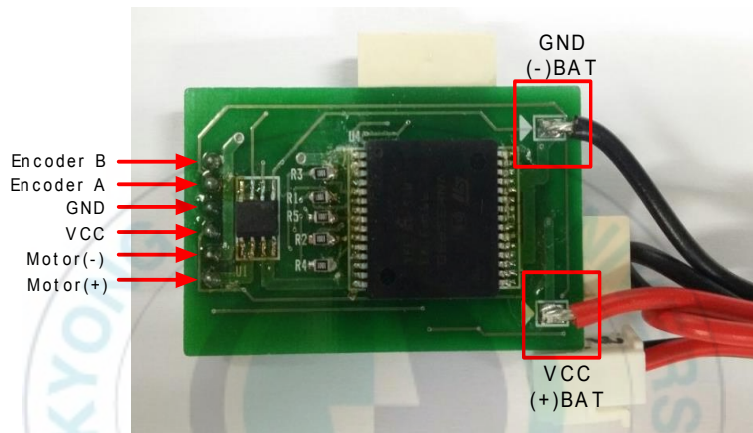


Fig. 5.9 Motor driver

Table 5.4 Specification of motor drive

Item	Specification
Operation Voltage	9V ~27V
Operation Current	Continuous 12A Burst 15A
Size	5cm(Width) x 3cm(Height length)
Communication	RS-232

5.2.4. Ultrasonic sensor

To calculate curvature of curved pipeline by measuring the distance from the sensor to the pipeline, ultrasonic sensor as shown in Fig. 5.10 is used. The specification of this sensor is listed in Table 5.5.

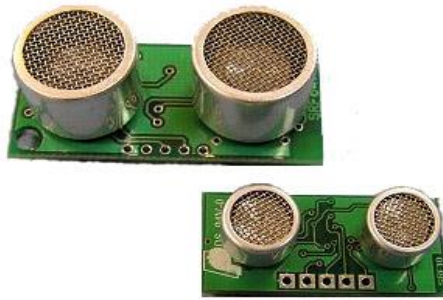


Fig. 5.10 Ultrasonic sensor SRF-10

Table 5.5 Specification of ultrasonic sensor

Item	Specification
Voltage	5v
Frequency	40 kHz type
Range	3cm – 6m
Communication	Standard I2C Bus

5.2.5. Driving DC motor

Driving DC motor IG-32RGM type for driving the developed PIR as shown in Fig. 5.11 is used and its specification is shown in Table 5.6.



Fig. 5.11 Driving motor IG-32RGM 05 Type

Table 5.6 Specification of driving DC motor

Item	Specification
Rated torque	1.0kg/cm ~ 12kg/cm
Rated rotational speed	950rpm ~ 8rpm
Motor	DC12V / 6.000rpm / 12.8W Motor
Encoder	26Pulses(13Pulses 2CH)

5.2.6. Angle sensor

Angle sensor is used to measure θ_{2i} of 4-bar linkage of the proposed pipe inspection robot in section 2.2. The sensor has a resistance of approximately 10 k Ω and can be operated at typical battery voltages to conserve power as shown in Fig. 5.12 and its specification is shown in Table 5.7.



Fig. 5.12 Angle sensor gaussmakov B10k Ω

Table 5.7 Specification of angle sensor

Item	Specification
Resistance	10k Ω
Supply Voltage	5.5 V
Port 1	Grand
Port 2	output
Port 3	VVC

5.2.7. Camera sensor

In this thesis, camera sensor, VIJE IP-2000 PT Wireless, is shown in Fig. 5.13 and its specifications in Table 5.8. Camera sensor with pan-tilt consists of camera sensor and pan-tilt is used to detect movement of the proposed pipe inspection robot.

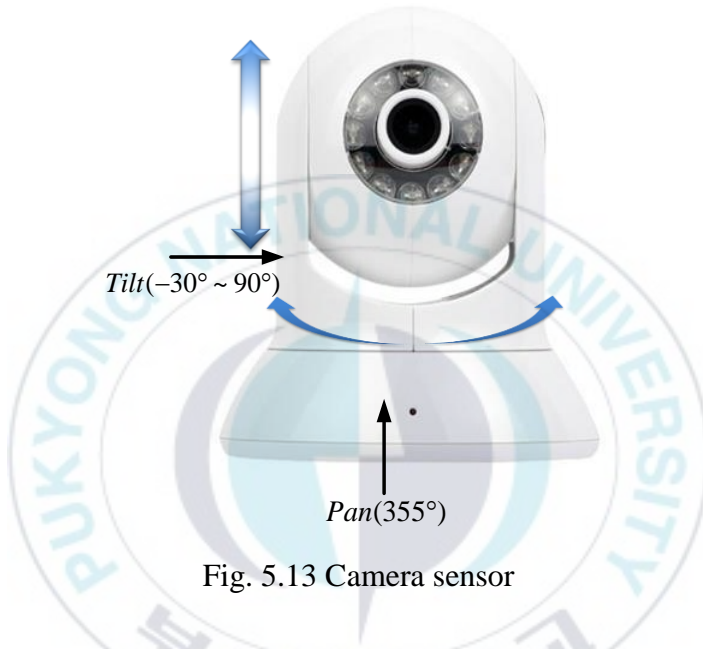


Fig. 5.13 Camera sensor

Table 5.8 Specification of camera sensor

Item	Specification
Resolution	1600 X 1200
Rotation	Left, Right 355° / Upper, Bottom -30 ~ 90°
Power Supply	12V DC Adapter
Network Protocol	TCP/IP, HTTP, SMTP, FTP, NTP, DNS, DDNS, DHCP, UPnP, RTSP, PPPoE, 3GPP

5.3. Proposed control system

A proposed control system of the proposed pipe inspection robot developed for this thesis is shown in Fig 5.14 and Table 5.9. The

control system consists of camera sensor (a), Host computer PC (b), Driving DC motor in active module (c), expansion DC motor (d), Ultrasonic sensor (e), Driving DC motor in passive module (f), RS-232 Bluetooth communication system (g) and encoder (h).

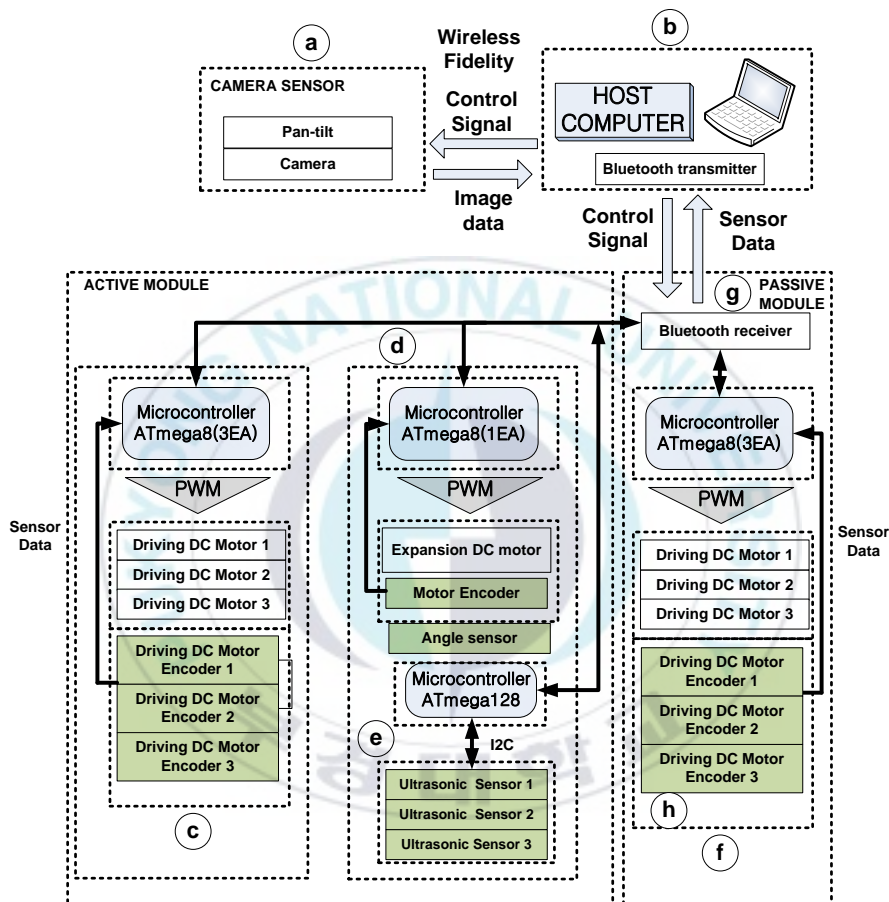


Fig. 5.14 Schematic block of the proposed control system

Table 5.9 Configuration of the propose control system

Simple	Name	Simple	Name
(a)	Camera Sensor,	(b)	Host computer
(c)	Driving DC motor and Microcontroller ATmega8 of active	(d)	Expansion DC motor, Angle sensor, microcontroller ATmega8

	module		of Active module
⑤	Ultrasonic Sensors and microcontroller ATmega128	⑥	Driving DC motor and microcontroller ATmega8 of passive module
⑦	RS232(Bluetooth)	⑧	Encoder

Functions of configuration of the proposed system shown in Fig. 5.14 and Table 5.8 are described as follows:

- ① *Camera sensor* : provide pan-tilt controlling camera sensor and installed in the center of front body of active module, obtain image data inside pipeline and transmit them to Host computer using wireless fidelity (WiFi) with communication .
- ② *Host computer* : transmit control command to drive the developed PIR through RS232 wireless communication and receive image data from all modules, and receive data obtained from camera sensor.
- ③ *Driving DC motor of active module*: drive active module by PWM signals received from ATmega8 (3EA)
- ④ *Expansion DC motor*: generate pressing force between 3 driving wheels and inner wall of pipeline by rotating thread shaft expanding and shrinking the 4- bar linkage of the active through the expansion DC motor.
- ⑤ *Ultrasonic sensor* : 3 ultrasonic sensors are installed in front body of active module, measure the distances from 3 ultrasonic sensors to inner wall of pipeline, transmit them to microcontroller ATmega128. Measured distances from curvature centers of 3 driving wheels to wheels are used to calculate reference angular velocities of 3 driving wheels.

⑦ *Driving DC motor of passive module* : drive passive module by PWM signals received from ATmega8 (3EA).

⑧ *RS-232 (Bluetooth)* : Connect Host computer with two microcontrollers kinds : One is a microcontroller ATmega8 for controlling driving DC motor, another is a microcontroller ATmega128 for measuring distance to inner wall using 3 ultrasonic sensors.

⑨ *Encoder*: 7 encoders are used for 3 driving DC motors of active module, one expansion DC motors and 3 driving DC motors of passive module.

5.4. Control process

For control process, C# AVR ATmega8 and AVR ATmega128 are used for GUI and motor driver control, respectively. Fig. 5.15 shows C# GUI to control only camera sensor and built-in software VIJE SAVITMICRO is used manually. There are five parts in the GUI, i.e. camera control panel, ① where users control the camera directions by pan-tilt, camera state window statement ② that displays the state of the current camera, slider window ③ that controls rotational speed by moving slider, camera vision information window ④ that displays the current state images of camera sensor, and a robot control panel ⑤ that rotates pan-tilt and camera sensor automatically and controls the robot motion.



Fig. 5.15 Graphic user interface

Fig. 5.16 shows ultrasonic sensor and a camera sensor installed in the active module. Three ultrasonic sensors are installed in parallel to three wheel direction spaced 120° from each other in front of the active module to measure distance from ultrasonic sensors to the pipe inner wall surface of pipeline using previous version. The camera sensor is installed in the front center of the body of the active module to investigate the condition of the pipe inner surface. The camera with pan-tilt is rotatable to the upper, lower, left, right 355° using (a) part indicated by a red dotted line in Fig. 5.15.

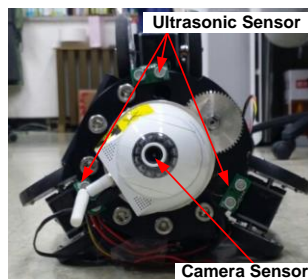


Fig. 5.16 Ultrasonic sensor and camera sensor

Fig. 5.17 shows GUI program (software) developed to control only the developed PIR using C# language. This GUI program controls driving DC motor and expansion DC motor save data of motor velocities and encoder and have function that power supply of the developed PIR turns off in emergency. The control panel for manual operation is shown in Fig. 5.17. There are three buttons, namely backward, stop, and forward. These buttons simply control the proposed PIR to move backward, stop and forward, respectively. The reference PWM value that is sent to motors is displayed at the three left bottom boxes, whereas the PWM value that is read by encoders is shown at the right bottom boxes ⑤, ⑥ and ⑦. Functions of buttons and windows shown in Fig. 5.17 are described as follows:

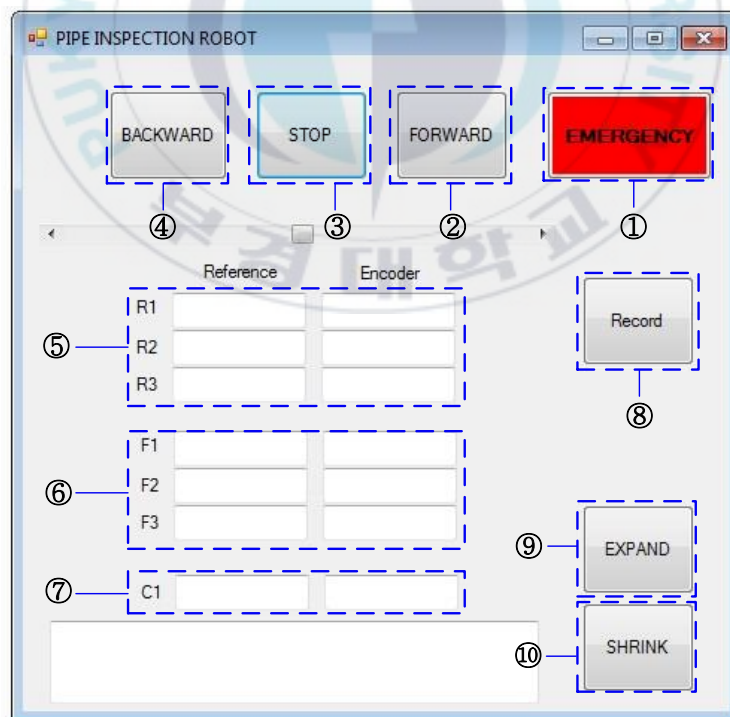


Fig. 5.17 Control panel for manual operation

- ① *EMERGENE*: Turn off all power of the developed PIR in emergency and stop the developed PIR.
- ② *FORWARD*: Increase linear velocities of 6 driving motors forward and increase 50 mm/s wherever the button is clicked once. With 5 steps, increase maximum 250mm/s.
- ③ *STOP*: Stop the developed PIR at a desired position of users during its movement.
- ④ *BACKWARD*: Increase linear velocities of 6 driving motors backward and increase 50 mm/s wherever the button is clicked once. With 5 steps, increase maximum 250mm/s.
- ⑤ *R1, R2, R3*: display angular velocities and encoder values of driving DC motor of passive module.
- ⑥ *F1, F2, F3*: display angular velocities and encoder values of driving DC motor of active module.
- ⑦ *C1*: display angular velocity and encoder value of expansion DC motor of active module.
- ⑧ *Record*: Save data of ⑤, ⑥, ⑦.
- ⑨ *EXPAND*: Expand 4-bar linkage to a desired position by rotating thread shaft using expansion DC motor of active module
- ⑩ *SHRINK*: shrink 4-bar linkage to a desired position by rotating thread shaft using DC motor of active module.

5.4.1. Universal joint

In this thesis, universal joint is shown in Fig. 5.18 and UNCA single type made of SSCM415 is used to joint active module and passive module together. And it can give more flexibility to drive in curved pipe and vertical pipe more naturally.



Fig. 5.18 Universal joint

5.4.2. Battery

In this thesis, two Lithium Polymer batteries as shown in Fig. 5.19, installed between body and active module and passive module for power respectively are used and their specification is shown in Table 5.10. It supplies voltage driving module, expansion DC motor, ultrasonic sensor, etc.



Fig. 5.19 Lithium polymer battery

Table 5.10 Specification of battery

Item	Specification
Size	146 X 50 X 24(mm)
Weight	291g
Voltage	11.1V
Maximum Charge Voltage	4.2V(Individual Cells)
Cut-off Voltage	40c ~ 70c(Max)

Chapter 6. Simulation and Experimental Results

6.1. Simulation results using the proposed diameter tracking controllers

Simulations are performed to verify the effectiveness of the conventional PI controller and the proposed fuzzy logic controller for diameter tracking. The parameter and initial values used in the simulation are listed in Table 6.1.

Table 6.1 Parameters and initial values of the i^{th} expansion DC motor

Parameter	Value	Unit	Parameter	Value	Unit
J_i	0.1	Kg m ²	l_i	150	mm
$K_{\phi i}$	0.4	J/A	l_{1i}	130	mm
b_i	0.02	Js/rad	l_{2i}	50	mm
R_i	3	Ω	l_{3i}	100	mm
L_i	0.13	H	r_{wi}	47.45	mm
$i_i(0)$	0	A	p_i	20	mm
$\theta_{mi}(0)$	0	rad/s	d_{1i}	95	mm
$\theta_{si}(0)$	5	deg	d_{2i}	75	mm
$\theta_m(0)$	0	rad			

By using the i^{th} expansion DC motor parameters in Table 6.1, matrices in Eq. (2.8) can be calculated as follows:

$$\mathbf{A}_i = \begin{bmatrix} -23 & -3 \\ 4 & -0.2 \end{bmatrix}, \quad \mathbf{B}_i = \begin{bmatrix} 7.6 \\ 0 \end{bmatrix}, \quad \mathbf{x}_i = \begin{bmatrix} i_{mi} & \dot{\theta}_{mi} \end{bmatrix}^T \quad (6.1)$$

Fig. 6.1 shows the simulation results of the radius tracking of the proposed pipe inspection robot by using two diameter tracking controllers such as the conventional PI controller and the fuzzy logic controller. Three reference radii are given as 0.15 m, 0.2 m and 0.25 m. For the conventional PI controller, the radii of the proposed PIR show overshoots of 0.013m, 0.018m, 0.061m when the proposed PIR are at inlets and outlets of the elbows and then converge slowly to the references. For the fuzzy logic controller, the radius of the proposed PIR converges to its references fast at 5s, 35s, and 65s when the proposed PIR are at inlets and outlets of the elbows. The results show that the proposed fuzzy logic controllers enables the radii of the proposed PIR to track the reference radii faster than the conventional PI controller. Fig. 6.2 shows the radius errors by both controllers. For the conventional PI controller, the radii of the proposed PIR show overshoots of 0.013m, 0.018m, 0.061m, and then converge slowly the references when the proposed PIR are at inlets and outlets of the elbows. For the fuzzy logic controller, the radius errors of the proposed PIR show the sudden sharp edges of -0.04 m, -0.05 m, 0.05 m when the proposed PIR are at the inlets and the outlets of the elbows and then converge to 0 m at 5s, 35s, and 65s. Fig. 6.3 shows control inputs for various walls using the conventional PI controller and the fuzzy logic controller. At points that the references are changed, both control inputs have sharp changes. The overshoots in the conventional PI controller makes the proposed PIR over-press to the inner walls of pipelines and cannot move smoothly, and can stop. The proposed fuzzy logic controller makes the proposed PIR to track its reference radii faster than the conventional PI controller.

Therefore, the fuzzy logic controller has better performance than the conventional PI controller because the proposed fuzzy controller makes the radius errors converge to zero faster than the conventional PI controller.

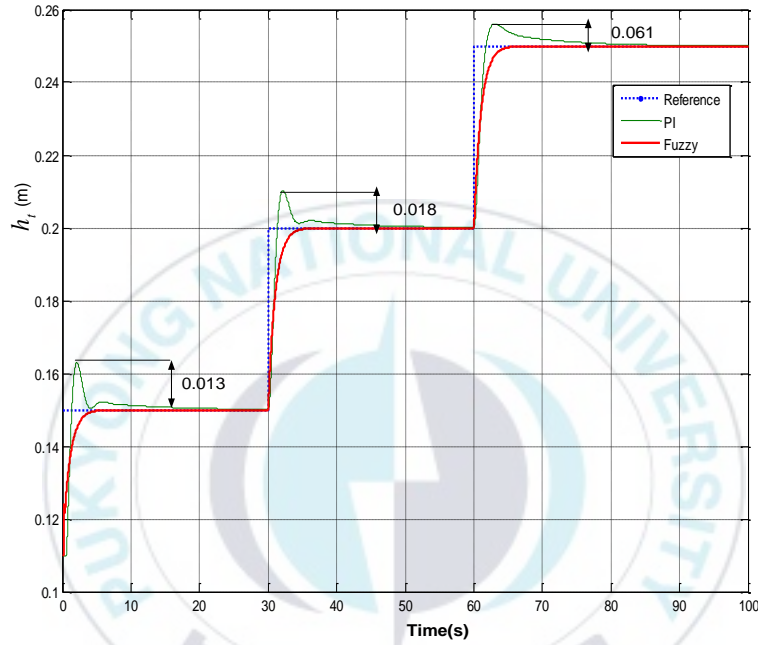


Fig. 6.1 Output radius h_i of the proposed PIR using both diameter tracking controllers

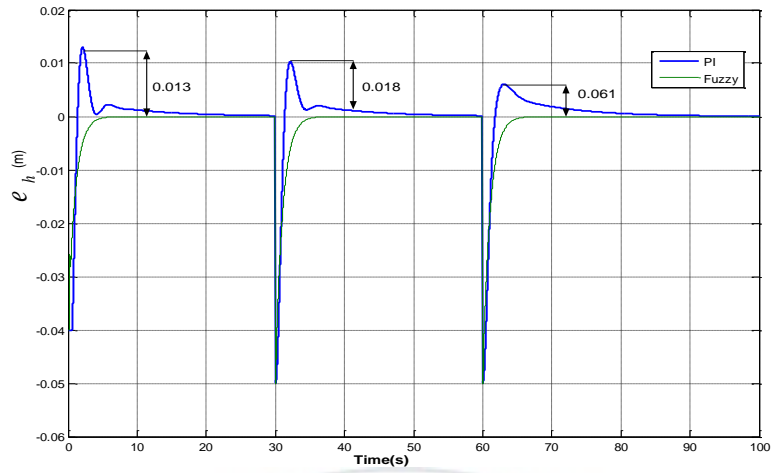


Fig. 6.2 Radius error e_h using the proposed PIR using both diameter tracking controllers

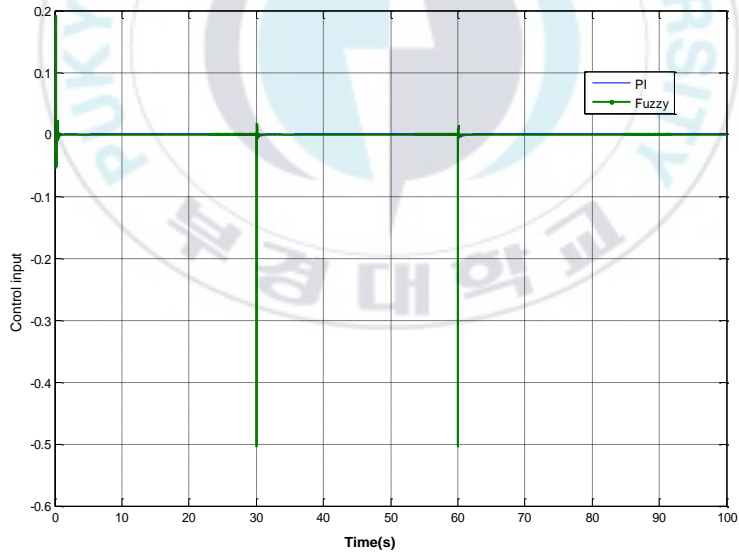


Fig. 6.3 Control input u of the proposed PIR using both diameter tracking controllers

6.2. Simulation results using the proposed driving controllers

Simulations are performed to verify the effectiveness of the conventional PI controller and the proposed fuzzy logic controller for tracking wheel reference velocities and reference PIR linear velocity inside a given pipeline. The pipeline used for simulation is shown in Fig. 6.4 and its dimension is shown in Fig. 6.5. Since the three driving DC motors that are used are the same, the motor parameters and initial values for simulation are same as listed in Table 6.2.

Table 6.2 Parameters and initial values

Parameter	Value	Unit
L_i	0.1	H
$K_{\phi i}$	0.3	J/A
J_i	0.1	Kg m ²
b_i	0.01	Js/rad
R_i	2	Ω
r_{wi}	45.25	mm
h_t	102.55	mm
i_m	$[0 \ 0 \ 0]^T$	A
$\dot{\theta}_a$	$[0 \ 0 \ 0]^T$	rad/s
r_{elbow}	457.2	mm

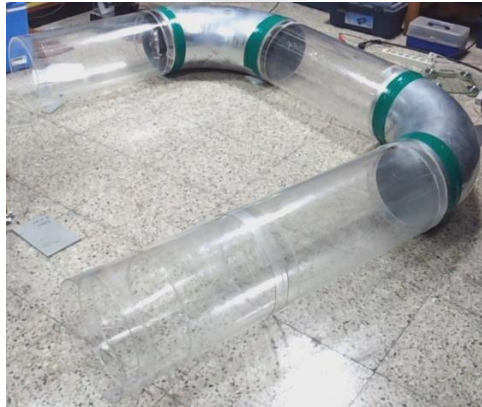


Fig. 6.4 Pipeline for simulation and experiment

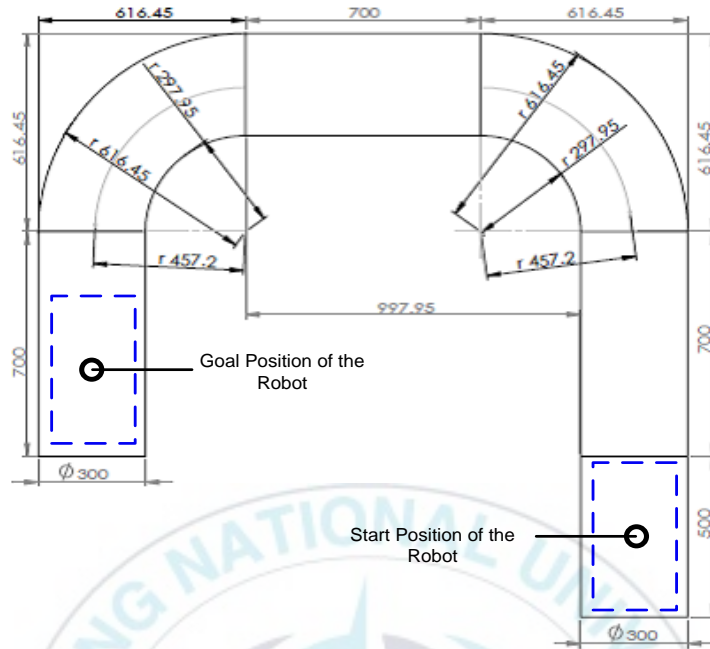


Fig. 6.5 Elbow and pipe specification (mm)

A_i and B_i in Eq. (2.21) from Table 6.2 are same for the three driving DC motors as follows:

$$A_1 = A_2 = A_3 = \begin{bmatrix} -20 & -3 \\ 3 & -0.1 \end{bmatrix}, B_1 = B_2 = B_3 = \begin{bmatrix} 10 \\ 0 \end{bmatrix}, \quad (6.2)$$

$$C_1 = C_2 = C_3 = \begin{bmatrix} 0 & 1 \end{bmatrix}$$

For the simulation with two controllers of the conventional PI controller and the proposed fuzzy logic controller, the PIR moves five paths, namely moving straight for 1200 mm, moving in elbows for 500mm, moving straight for 457.2mm, moving in elbows for 700mm, and finally moving straight for 700 mm. Nominal linear velocity of the PIR v_{cz} is 178mm/s and is used as reference in the simulation.

Therefore, when the PIR moves in elbows ($r_{elbow} = 457.2\text{mm}$), the reference angular velocities ω_{rx} , ω_{ry} of the PIR are

$$\omega_{rx} = \frac{v_{cz}}{r_{elbow}} = \frac{178\text{mm/s}}{457.2\text{mm}} = 0.39\text{rad/s} \quad (6.3)$$

$$\omega_{ry} = 0\text{rad/s} \quad (6.4)$$

Figs. (6.6) ~ (6.15) show the simulation results. The results show that the two controllers of the conventional PI controller and the proposed fuzzy logic controller enable the PIR to follow the reference velocities very well. Fig. 6.6 and Fig. 6.7 show the simulation results of angular velocities and angular velocity errors of the PIR with respect to x axis. These figures show that the PIR follows the reference wheel angular velocities of 0 rad/s in straight pipeline and of 0.39 rad/s in elbow very well by both controllers. The proposed fuzzy logic controller makes the angular velocities of the PIR in x direction change to its reference velocities faster than the conventional PI controller. Fig. 6.8 shows the simulation result of the angular velocities of the proposed PIR with respect to y axis by both controllers. Since the PIR does not move in vertical direction, its reference angular velocity with respect to y axis is 0 rad/s. Both controllers make the proposed PIR have about -0.0022 rad/s at the inlets and the outlets of curved pipelines, (elbow), where the references are changed and then converge to its reference of 0 rad/s. However, the proposed fuzzy controller makes errors converge to zero faster than the conventional PI controller. Fig. 6.9 shows

simulation results of wheel angular velocity errors of the proposed PIR with respect to y axis by both controllers. The sharp changes of 0.0022 rad/s that appear in the figures occur when the PIR is at the inlets and the outlets in the elbows by both controllers. Simulation results for the PIR linear velocity is shown in Fig. 6.10. This figure shows that the PIR can track the reference linear velocity of 178 mm/s very well by both controllers. The proposed fuzzy controller converges to its reference faster than the conventional PI controller. Fig. 6.11 shows simulation results of linear velocity error by both controllers. The fuzzy logic controller makes the linear velocity error of the proposed PIR converge to zero faster than the conventional PI controller. Fig. 6.12 shows the angular velocities of three wheels of the proposed PIR. It shows that the wheel angular velocity of wheel 1 is same to 3.8 rad/s for the straight pipelines and elbows and 3 wheels have different angular velocities for the curved pipelines. The angular velocities in wheel 1 are 3.8 rad/s, and the angular velocities in wheel 2 and wheel 3 are $\dot{\theta}_2 = 4.5$ rad/s and $\dot{\theta}_3 = 3.1$ rad/s by both controllers. Therefore, the proposed PIR turns from the wheel 2 to wheel 3. At the inlets and the outlets of the elbow, the proposed fuzzy logic controller makes the proposed PIR converge to the reference wheel angular velocities faster than the conventional PI controller. Figs. 6.13 ~ 6.15 show the simulation results of wheels angular velocity errors of wheel 1, wheel 2 and wheel 3, respectively. The wheel angular velocity error of the wheel 1 converges to zero at about 1 second for proposed fuzzy logic controller and at about 3 second for the conventional PI controller. The angular velocities of wheel 2 show the sharp errors of ± 0.7 rad/s occurs in the inlets and the outlets of elbows and then converge to zero. The wheel 3 has the

reverse states of wheel 2. The proposed fuzzy logic controller makes the proposed PIR converges to the reference PIR linear velocity and reference wheel angular velocities faster than the conventional PI controller.

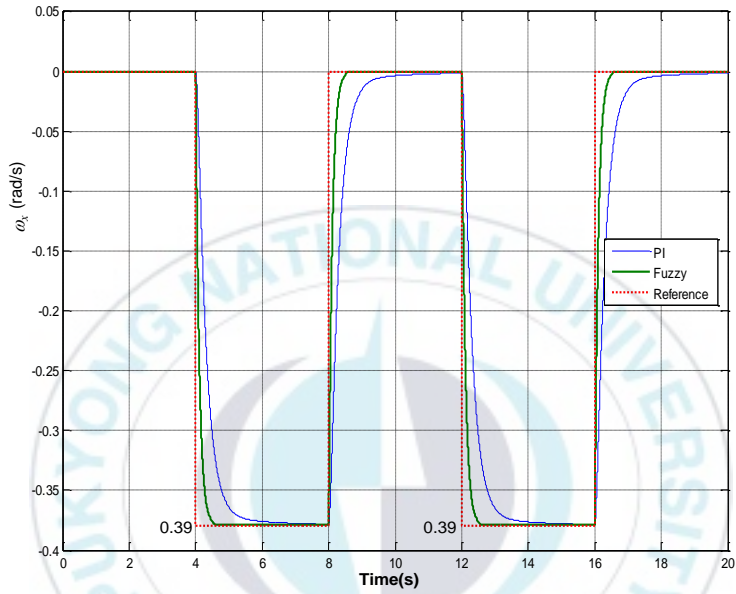


Fig. 6.6 Angular velocity of the proposed PIR with respect to x axis

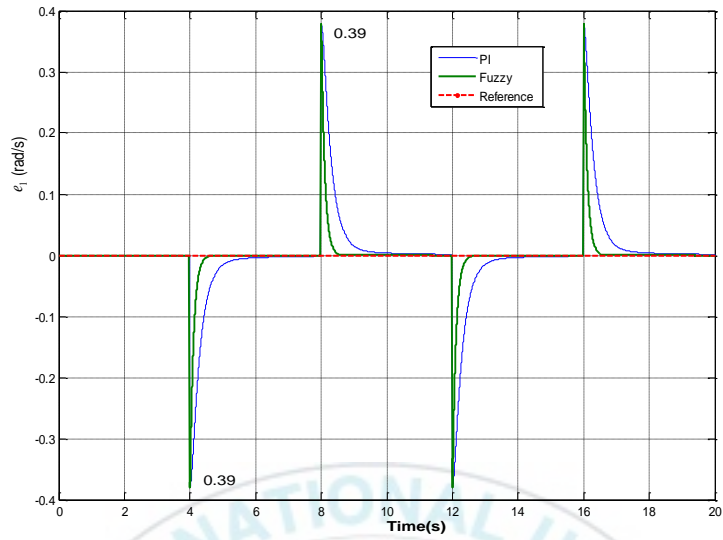


Fig. 6.7 Angular velocity error of the proposed PIR with respect to x axis

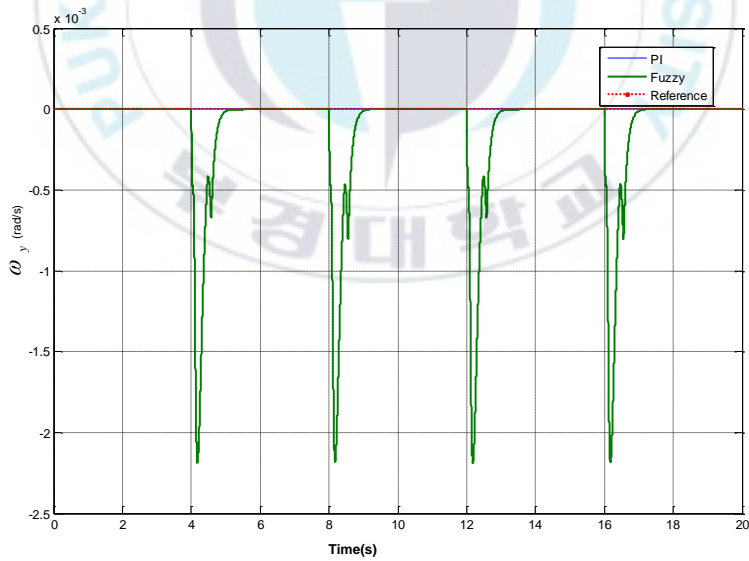


Fig. 6.8 Angular velocity of the proposed PIR with respect to y axis

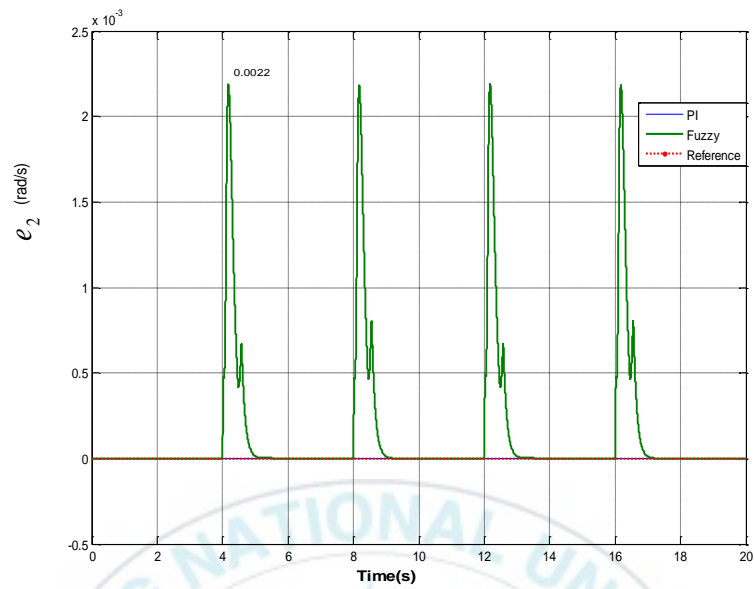


Fig. 6.9 Angular velocity error of the proposed PIR with respect to y axis

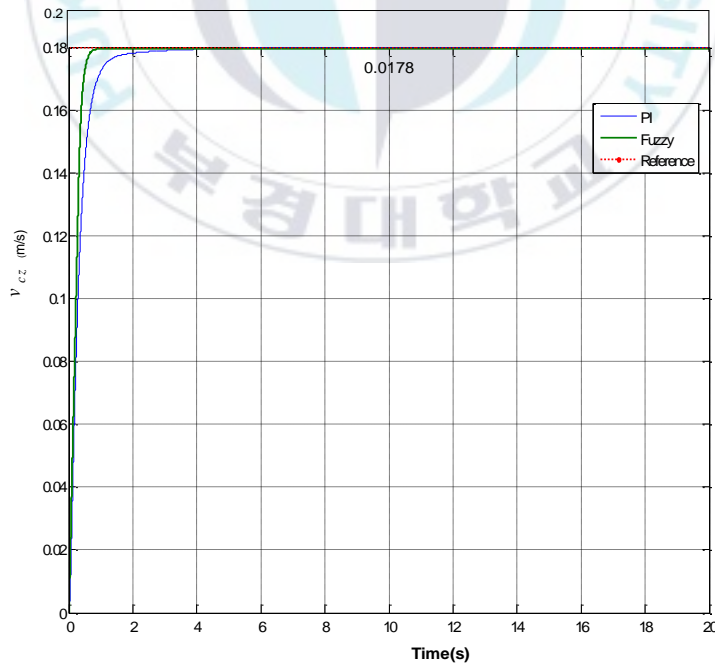


Fig. 6.10 Linear velocity of the proposed PIR

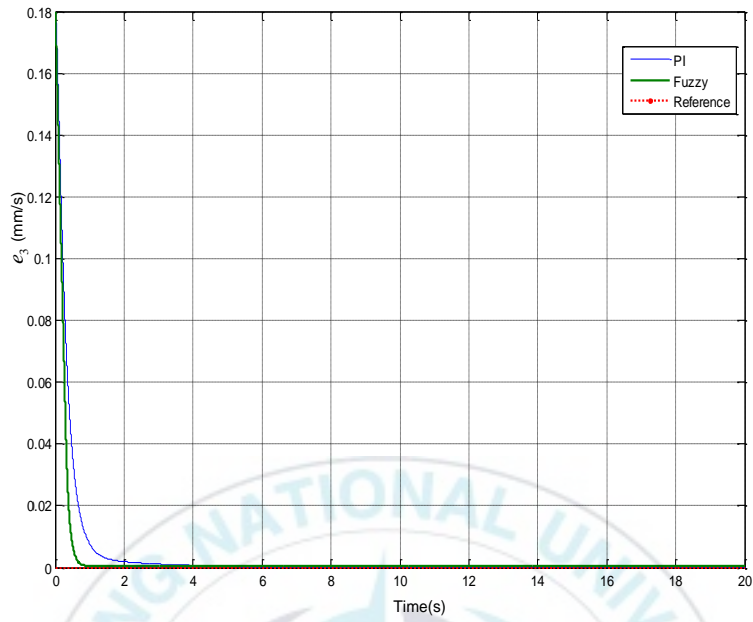


Fig. 6.11 Linear velocity error of the proposed PIR

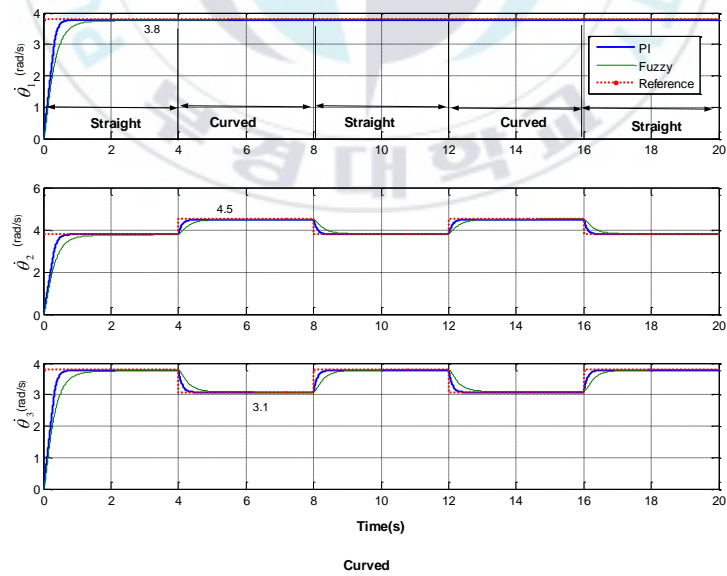


Fig. 6.12 Wheel angular velocities

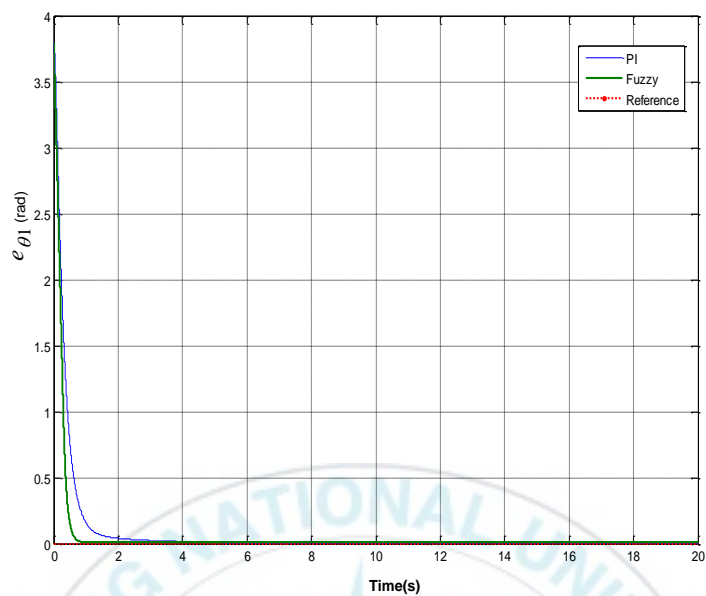


Fig. 6.13 Wheel angular velocity error $e_{\theta 1}$

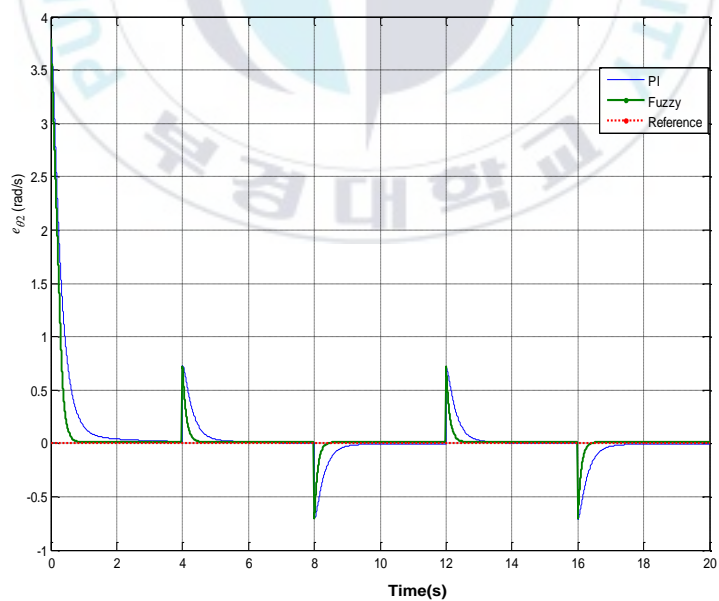


Fig. 6.14 Wheel angular velocity error $e_{\theta 2}$

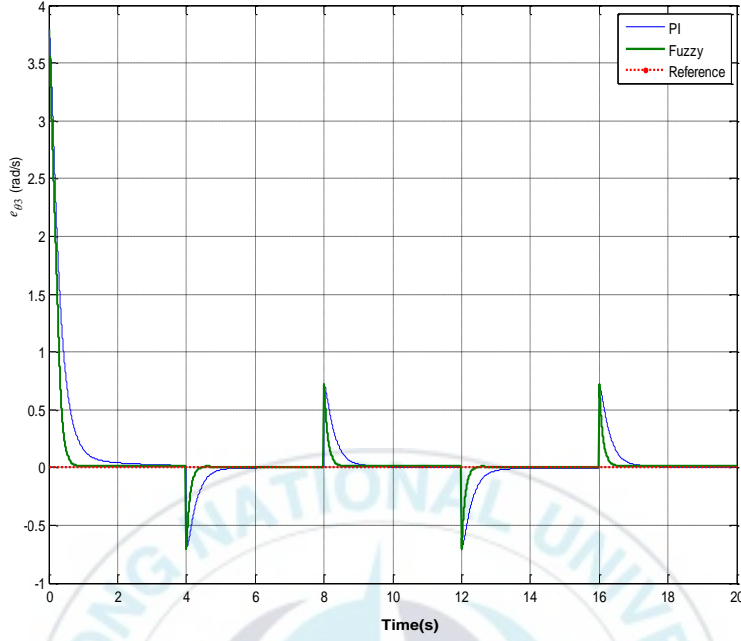


Fig. 6.15 Wheel angular velocity error e_{θ_3}

6.3. Experimental results for driving control

This section shows the experimental results performed to verify the driving control performance of the conventional PI controller and the proposed fuzzy logic controller for the proposed pipe inspection robot. The experiments are conducted by making the proposed PIR track the reference velocities. The experimental results show that the conventional PI controller and the proposed fuzzy logic controller enable the PIR to drive inside the pipeline successfully by tracking the reference velocities in horizontal straight pipeline and elbow. Figs. 6.16 ~ 6.25 shows the reference values and the experimental results of the conventional PI controller and the proposed fuzzy logic controller for tracking the wheel reference velocities and the

reference PIR linear velocity inside a given pipeline. Fig. 6.16 represents the experimental angular velocities of the proposed PIR with respect to x axis by both controllers. The proposed PIR moves 5 paths such as driving in the straight pipeline for 0–4 seconds, driving in the curved pipeline for 4–8 seconds, driving in straight pipeline for 8–12 seconds, driving in the curved pipeline in the curved pipeline for 12–16 seconds, and driving from 16 to 20 seconds by both controllers mentioned in section 6.2. Both controllers make the experimental angular velocities of the proposed PIR with respect to x axis track its reference angular velocities. However, the proposed fuzzy logic controller makes the experimental angular velocities of the proposed PIR with respect to x axis converge to its reference angular velocities faster in both straight pipeline and curved pipeline than the conventional PI controller. Fig. 6.17 shows the experimental angular velocity error of the PIR in the x axis. The experimental errors at the inlets and outlets of the curved pipeline show sharp values ± 0.3 rad/s by both controllers. However, the proposed fuzzy logic controller makes the errors converge to 0 rad/s faster than the conventional PI controller.

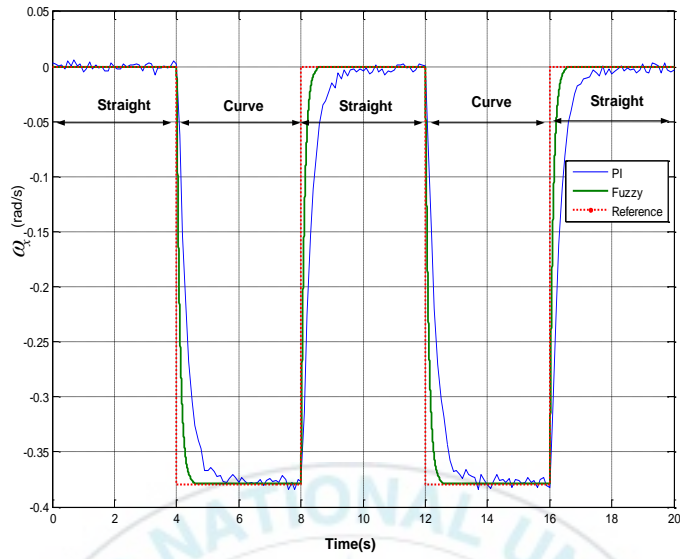


Fig. 6.16 Experimental angular velocity of the proposed PIR with respect to x axis

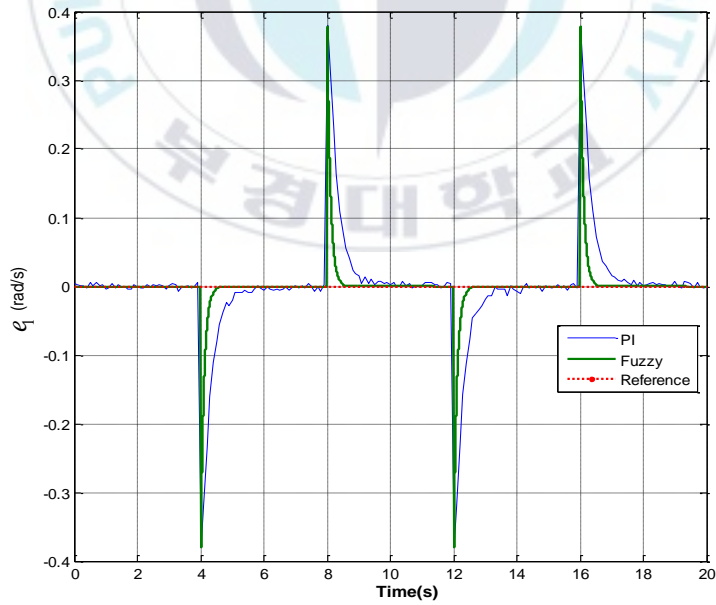


Fig. 6.17 Experimental angular velocity error of the proposed PIR with respect to axis

Figs. 6.18 and 6.19 represent the experimental angular velocity and the experimental angular velocity error of proposed PIR with respect to y axis, respectively. The experimental angular velocities of the proposed PIR with respect to y axis show about 0.0022 rad/s for the proposed fuzzy logic controller in both the inlets and the outlets of the curved pipelines. They are with $-0.009 \sim 0.008$ rad/s in straight and curved pipelines for the conventional PI controller. The experimental angular velocity shows $-0.002 \sim 0$ rad/s for the fuzzy logic controller and $-0.008 \sim 0.009$ rad/s for conventional PI controller.

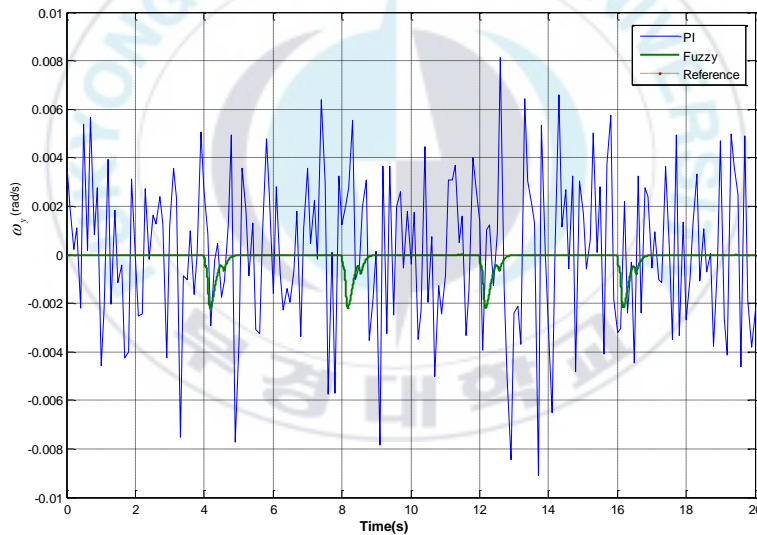


Fig. 6.18 Experimental angular velocity of the proposed PIR with respect to y axis

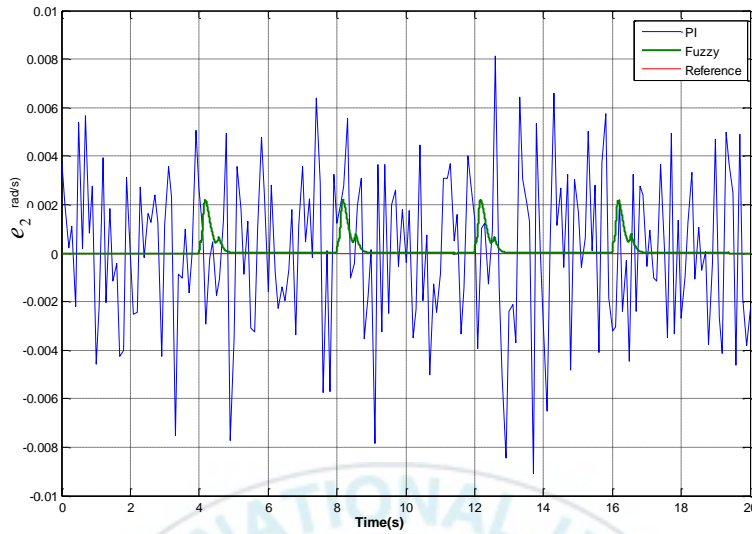


Fig. 6.19 Experimental angular velocity error of the proposed PIR with respect to y axis

Figs. 6.20 and 6.21 show the experimental results of the linear velocity and the linear velocity error of the proposed PIR. The proposed PIR tracks also the reference linear velocity of (178 mm/s) at about 1 second for the proposed fuzzy logic controller, and 2 seconds for the controller PI controller, however, the proposed PIR tracks reference at about 2 second has its experimental linear velocity of $0.178 \pm 0.006 \text{ m/s}$ for the conventional PI controller. However, the proposed PIR tracks its reference at about 2 second and experimental linear velocity for the conventional PI controller. Fig. 6.21 shows that the experimental error of the proposed PIR converges to zero at about 1 second for fuzzy logic controller and about 2 seconds for the conventional PI controller. Fig. 6.22 shows the experimental results of the wheel angular velocities of the proposed PIR by both controllers. The experimental wheel angular velocity of wheel 1

tracks its reference of 3.8 rad/s in straight pipelines and curved pipelines. The experimental wheel angular velocities of wheel 2 and wheel 3 track its reference of 4 rad/s in straight pipeline and has 4.5 and 3.1 rad/s in curved pipeline, respectively. However, the proposed fuzzy logic controller makes the experimental wheel angular velocities of 3 wheels converge their references faster than the conventional PI controller. Figs. 6.23 ~ 6.25 show the wheel angular velocity errors of the proposed PIR by both controllers. The angular velocity error of wheel 1 converges to zero at about 2 seconds for the conventional PI controller. The angular velocity error of wheel 2 has ± 0.7 rad/s at the inlets and outlets of the curved pipelines where the references are changed and then converge to zero. However, the fuzzy controllers make the errors converge to 0 rad/s faster than conventional PI controller. The error of wheel 3 has the reverse state wheel 2.

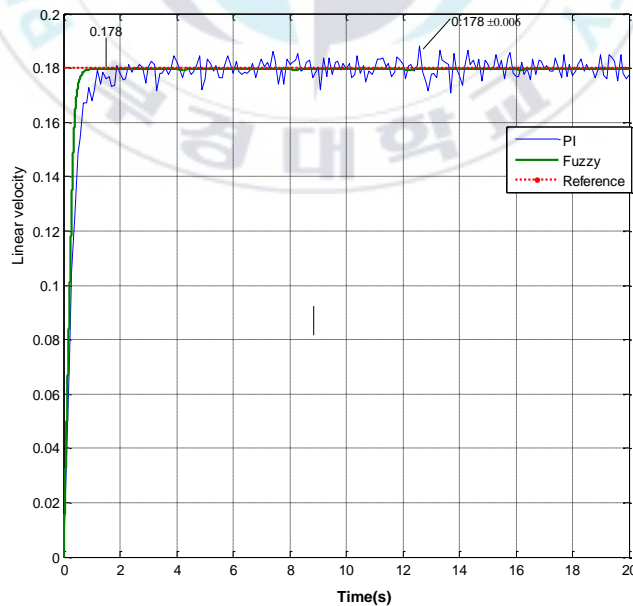


Fig. 6.20 Experimental linear velocity of the proposed PIR

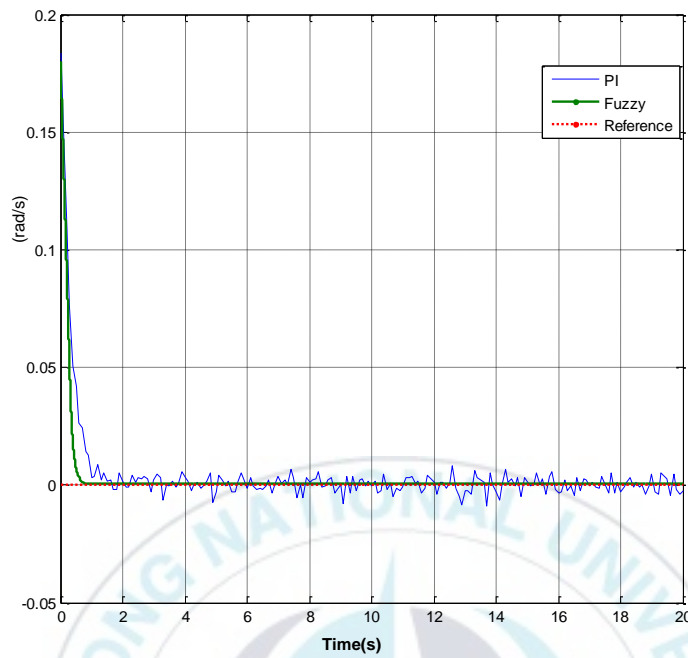


Fig. 6.21 Experimental linear velocity error of the proposed PIR

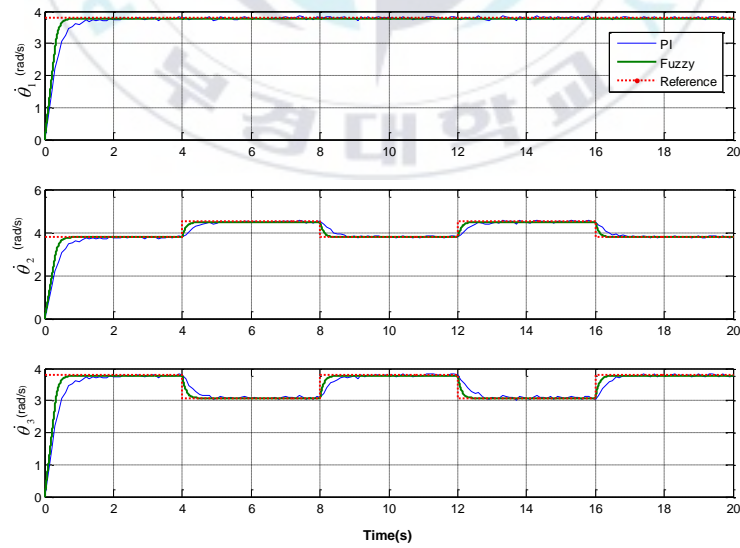


Fig. 6.22 Experimental wheel angular velocities

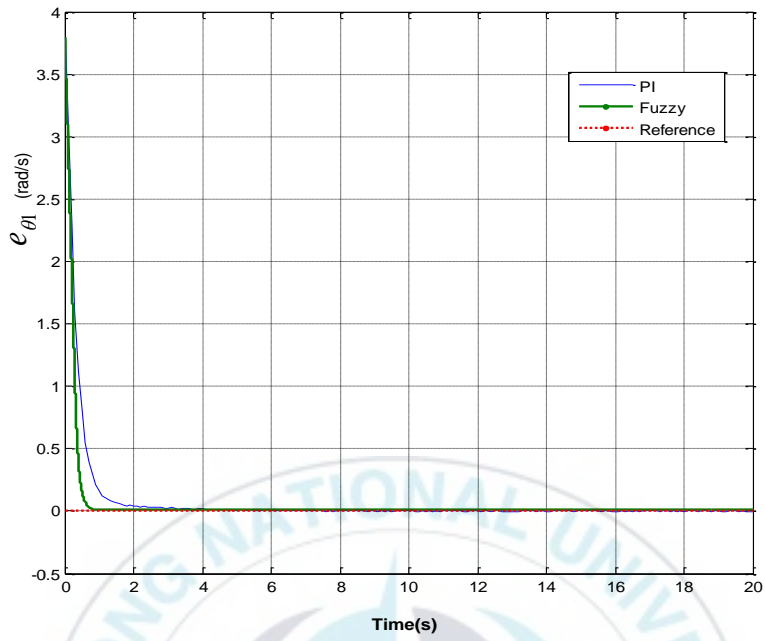


Fig. 6.23 Experimental wheel angular velocities error $e_{\theta 1}$

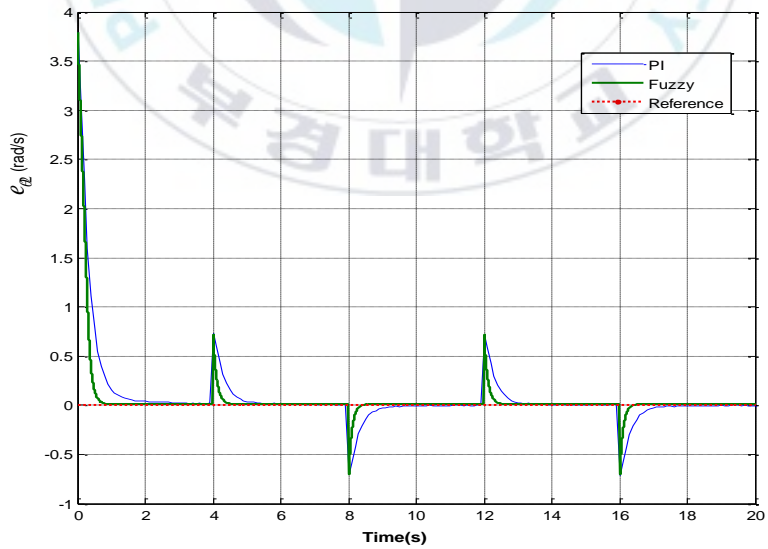


Fig. 6.24 Experimental wheel angular velocities error $e_{\theta 2}$

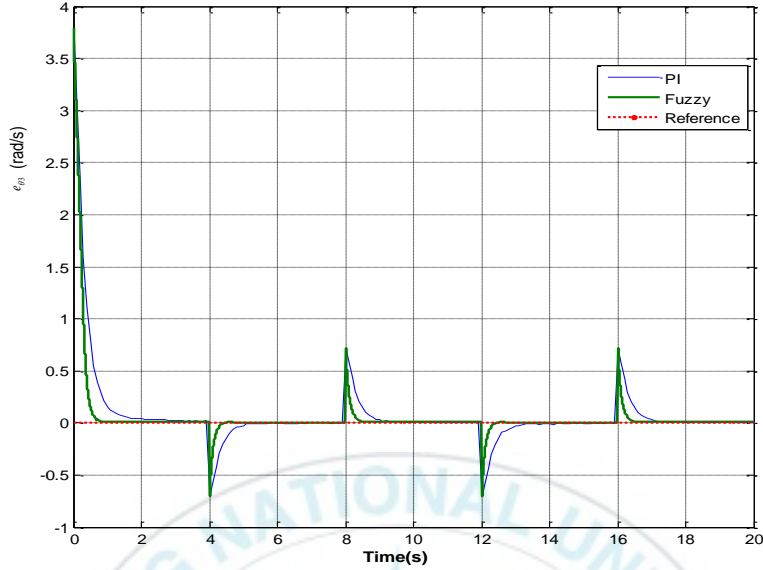


Fig. 6.25 Experimental wheel angular velocities error e_{θ_3}

Fig. 6.26 shows the distance measurement data inside the pipeline with $\phi 300$ mm. Measured data are obtained by measuring the distance to pipe wall using 3 ultrasonic sensors. Measured distance values of the 3 ultrasonic sensors are defined as I_p, I_q, I_r . “In” points in this figure represent the inlets of the curved pipelines. Therefore, through the experiment, this figure shows that the inlets of the curved pipelines have values of $\alpha = 500$ mm. The proposed PIR has the driving in straight pipeline and detects curved pipelines in its fronts for 0-4 seconds. By approaching the curved pipelines more, α has lower values. At 4 seconds, the proposed PIR acknowledges judging its entering the curved pipelines. It drives in the curved pipeline for 4-8 seconds by the driving algorithm based 3 ultrasonic sensors. In this case, the sensor values increase while the proposed PIR passes through the curved pipeline. For 8-12 seconds, the proposed PIR

passes through the curved pipeline, pass through straight pipelines, and detects the curved pipeline in its front and the sensor value decreases gradually. For 12-16 seconds, the proposed PIR re-drives in the curved pipelines. After 16 seconds, because there is no curved pipeline and no wall in its front, the sensor value is not changed. When the proposed PIR enters the curved pipeline at 4 seconds and 12 seconds, the values of 3 ultrasonic sensors have $I_p > I_q > I_r$. It means that the direction of the curved pipe is the same direction of I_q .

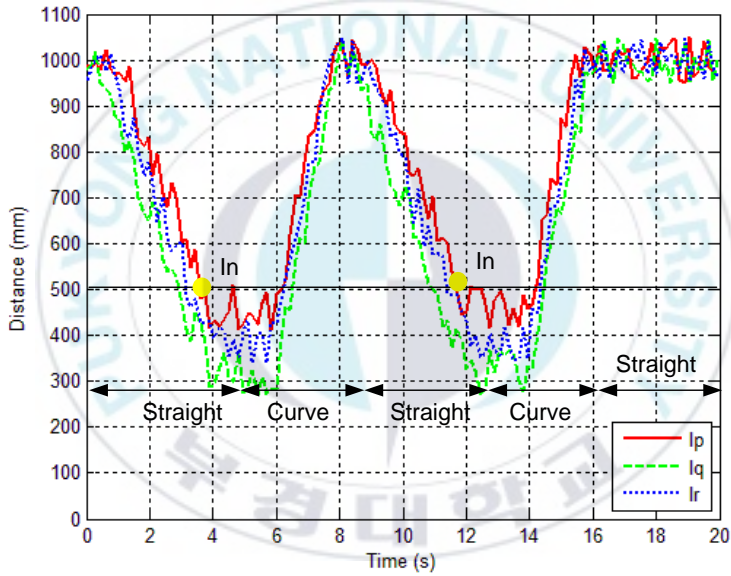


Fig. 6.26 Experimental ultrasonic sensor data (I_p , I_q , I_r)

Fig. 6.27 shows driving presses with 5 steps mentioned in section 6.2 of the such as straight pipeline (a) → elbow (b) → straight pipeline (c) → elbow (d) → straight pipeline. (a) shows the straight driving process in straight pipeline by controlling so that 3 wheel velocities of the proposed PIR are same. In (b), the proposed PIR acknowledges entering the curved pipeline through the ultrasonic

sensors and the 3 ultrasonic sensors is used to check the curvature and the direction of the curved pipe. In (c), the velocity of each wheel is calculated to pass through the curved pipe smoothly by the proposed driving algorithm and the velocity of each wheel is controlled to track the calculated velocity by the proposed driving algorithm using the fuzzy logic controller. In (d), the proposed PIR has passed through the curved pipeline and drives straight pipelines with controlling the velocities of 3 wheels to be same. In (e) → (f), the (a) ~ (d) processes are repeated to drive the curved pipeline. Experimental results show that smooth driving inside the straight pipelines and the curved pipeline was possible and the performance of the proposed controller is verified. At these times, the proposed PIR can drive stably with keeping the pressing force to the inner wall of pipelines by the active module and the passive module.

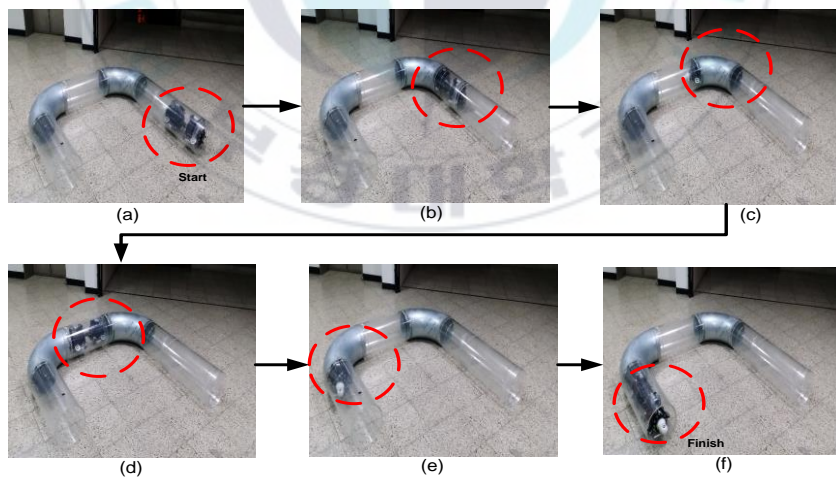


Fig. 6.27 Driving experiments in the pipeline

6.4. Driving test result using the fuzzy logic controller

Fig. 6.28 shows images taken by the camera sensor while the proposed PIR drives inside the given pipeline using the fuzzy logic controller. (a) shows the image of the inner wall state taken by the camera sensor at the inlets of pipelines. (b) shows the image of state curved pipeline taken by the camera sensor and it means that the proposed PIR enters the curved pipeline. (c) shows the image of the inner wall state of the curved pipeline. (d) shows the image taken by the camera sensor while the proposed PIR drives inside curved pipeline just before the proposed PIR leaves the curved pipeline. Finally, (e) shows the image taken by the camera sensor when the proposed PIR meets the straight pipeline.

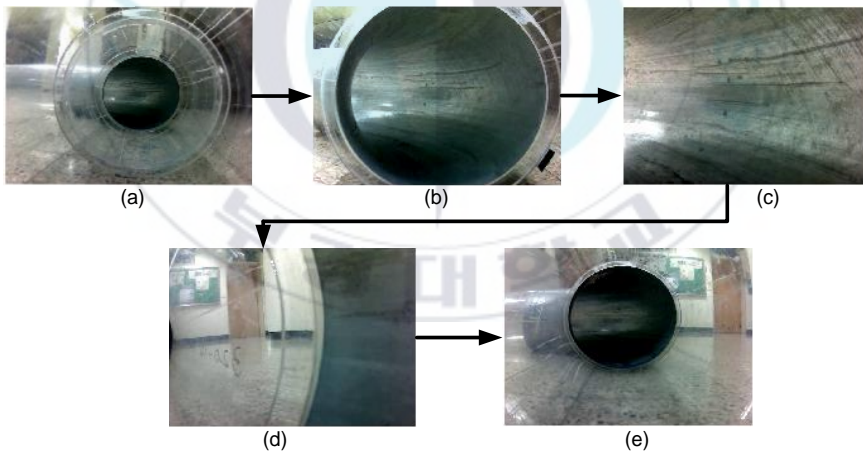


Fig. 6.28 Images of the pipeline state taken by the camera sensor during driving test

Chapter 7. Conclusions

7.1. Conclusions

This thesis proposed two controllers such as a diameter tracking controller for a wheeled type of pipe inspection robot to adjust its diameter automatically and a driving controller to drive to inside the pipelines with diameters from 300 to 500 mm using a fuzzy logic controller and a conventional PI controller. Conclusions of this thesis were summarized as follows:

- The developed PIR consisted of two modules, namely active module and passive module, and universal joint for the connection of two modules. It had 7 DC motors such as 3 driving DC motors for active module, 3 driving motors for passive module and one expansion DC motor for expanding 4-bar linkage in active module and spring in passive module for generating pressing force toward the wall of a pipeline.
- Kinematic modeling of 4-bar linkage of the active module and dynamic modeling of the expansion DC motor to track the reference diameter are proposed. In addition, kinematic modelings of the proposed PIR are proposed and dynamic modelings of the driving DC motor for driving inside the pipelines are proposed.
- Because it's active module enabled the proposed PIR to automatically adjust its radial dimension between 150-250 mm to attach to the inner wall pipelines with different inner diameters. It could travel through pipelines with varying inner diameters.
- A driving algorithm was proposed for the developed PIR to drive smoothly inside the curved pipeline. The driving algorithm was to

decide 3 reference wheel angular velocities and reference PIR linear velocity by measuring the distances to inner wall using 3 ultrasonic sensors to calculate the curvature and the direction of the curved pipeline.

- A conventional proposed PI controller and a fuzzy logic controller based on the kinematic modeling of the 4-bar linkage and the dynamic modeling of expansion the DC motor are designed for the proposed PIR to track given reference diameters of pipelines with different diameters by making the tracking errors.
- The hardware structure and software for a control system of the proposed PIR developed to implement the proposed controllers was described. The system was comprised of mechanical part design such as bodies of the active module and passive module and 6 wheel configurations and electronic part design such as industrial, DC motors, encoders, batteries, microcontroller AVR Atmega128, and Atmega8, motor drivers, angle sensor, ultrasonic sensors, and wireless camera. The developed GUI software program to control the developed PIR was described.
- Simulations were conducted to verify the effectiveness performances of the proposed two diameter controllers such as a fuzzy logic controllers and conventional PI controller. However, the simulation result should that the fuzzy logic controller made radii of the developed PIR converge to reference radii faster than that of conventional PI controller to track given reference diameters 0.15 m, 0.2 m, 0.25 m of pipelines. At the inlets and the outlets of the curved pipelines where the references were changed, they had sharp values and then converged to their references. In addition, simulations were conducted to verify the effectiveness of

the proposed two driving controllers such as a fuzzy logic controller and a conventional PI controller. The simulation results showed that the proposed two controllers could make the developed PIR follow its reference velocities obtained from the proposed driving algorithm inside a given pipeline in the experimental environment with horizontal straight and curved pipelines with different diameters and elbows. However, simulation results showed that the proposed fuzzy logic controller made the angular velocities of 3 wheels and the PIR linear velocity track its reference wheel velocities and its linear velocity faster than the conventional PI controller. The simulation result of the angular velocity of the proposed PIR with respect to x axis tracked 0.39 rad/s in elbow and 0 rad/s in straight pipeline well by both controllers.

- The angular velocity with respect to y axis tracked its reference of 0 rad/s and its errors showed 0.0022 rad/s. The linear velocity of the proposed PIR tracked its reference of 178 mm/s by both controllers. The angular velocities of 3 wheels tracked their references of 3.8 rad/s in straight pipelines and $\dot{\theta}_1 = 3.8$ rad/s, $\dot{\theta}_2 = 4.5$ rad/s, $\dot{\theta}_3 = 3.1$ rad/s in curved pipelines well by both controllers. However, the fuzzy logic controller tracked their references faster than the conventional PI controller. Thus, the overall results showed that the simulations tracked the reference values well by both controllers.
- Experimental results were to verify the performance of two controllers such as the proposed fuzzy logic controller and conventional PI controller for the developed PIR to track its

reference wheel velocities and its reference linear velocity obtained from the proposed driving algorithm inside a given pipeline with different diameters combined straight pipeline and elbows. The angular velocity of the proposed PIR with x axis tracked its reference of 0.39 rad/s by both controllers and the angular velocity of y axis was bounded within $-0.008 \sim 0.0009$ rad/s and its error was bounded within $-0.009 \sim 0.008$ rad/s in straight and curved pipelines for the conventional PI controller. The angular velocity of the proposed PIR with respect to y axis for the fuzzy logic controller was bounded near 0 rad/s in straight pipelines, and had sharp edges of 0.0022 rad/s and then converges to zero. Both controllers enabled the PIR to drive inside the pipeline successfully by tracking the reference velocities in horizontal straight pipeline and elbow and the linear velocity of the PIR for the fuzzy controller converged to its reference of 0.178 m/s at 1 second and its linear velocity was bounded within 0.178 ± 0.006 m/s for the conventional PI controller. The experimental angular velocities of 3 wheels tracked their references in straight pipelines and curved pipelines well by both controllers. The angular velocity of wheel 1 tracked its reference of 3.8 rad/s in straight and curved pipelines, and the angular velocities of wheel 2 and wheel 3 tracked their references of 4.5 rad/s and 3.1 rad/s in curved pipelines, respectively. Therefore, the experimental results tracked their references well.

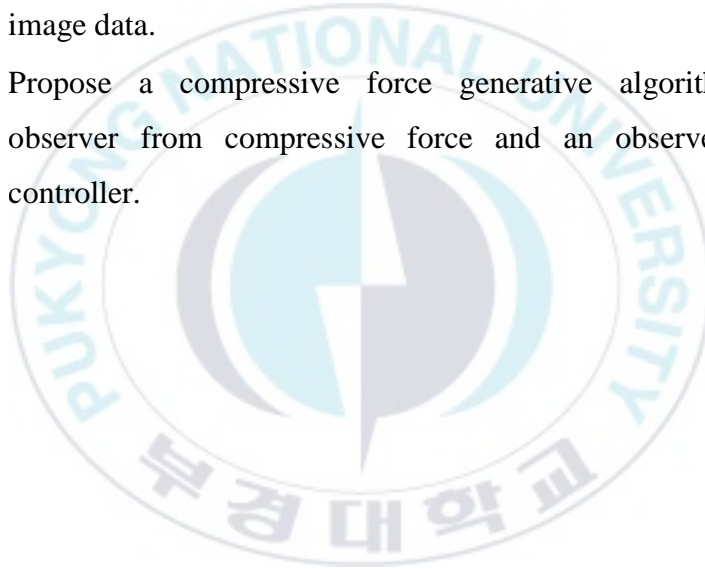
- Finally, the applicability and effectiveness of the developed PIR were verified by taking image of the inner state of pipelines in real time during the pipe inspection.

The developed PIR of developed in this thesis are expected to be able to contribute to the inspection of pipelines used in a variety of industrial applications such as power plant, and ocean plant, etc.

7.2. Future Works

The future works for this thesis are as follows:

- Apply small window algorithm to reduce the noise to get the image data.
- Propose a compressive force generative algorithm, an observer from compressive force and an observer-based controller.



References

- [1] 박철한, 김학경, 김상봉, “가변형 배관에 적응하기 위한 배관 탐사로봇의 개발”, 한국마린에너지어링학회 공동학술대회 논문집, pp. 279~280, 2010.
- [2] 박영우, 김윤종, 윤경현, “다양한 배관크기에 적용가능한 배관탐사로봇의 개발(Development of the Pipe-Inspection Robot for Various Sizes)”, 한국정밀공학회 2009년도 춘계학술대회 논문집, pp. 719~720, 2009.
- [3] T. S. N. Saga and T. Nakamura, “*Development of a Peristaltic Crawling Robot Using Magnetic Fluid on The Pasic of the Locomotion Mechanism of The Earthworm*”, Smart Materials and Structures, Vol. 13, pp. 566~ 569, 2004.
- [4] F. Kirchner and J. Hertzberg, “*A Prototype Study of an Autonomous Robot Platform for Sewerage System*”, Autonomous Robots, Vol. 4, No. 4, pp. 319~331, 1997.
- [5] H. B. Kuntze and H. Haffner, “*Experiences with the Development of a Robot for Smart Multistep Sonic Pipe Inspection*”, IEEE International Conference on Robotic and Automation, pp. 1773~1778, 1998.
- [6] S. G. Roh and H. R. Choi, “*Differential-drive In-pipe Robot for Moving Inside Urban Gas Pipelines*”, IEEE Transactions on Robotics, Vol. 21, No. 1, pp. 1~17, 2005.
- [7] M. Muramatsu, N. Namiki, R. Koyama and Y. Saga, “*Autonomous Mobile Robot In pipe for Piping Operations*”, IEEE/RSJ International Conference on Intelligent Robots and Systems, Vol. 3, pp. 2166 ~2171, 2000.

- [8] M. Moghaddam and M. R. Tafti, "*Design, Modeling and Prototyping of a Pipe Inspection Robot*", 2nd International Symposium on Automation and Robotics in Construction (ISARC), 2005.
- [9] Y. Zhang and G. Yan, "*In-pipe Inspection Robot with Active Pipe-diameter Adaptability and Automatic Reactive Force Adjusting*", Mechanism and Machine Theory, Vol. 42, pp. 1618~1631, 2007
- [10] H. R. Choi and S. M. Ryew "*Robotic System with Active Steering Capability for Internal Inspection of Urban Gas Pipelines*", Mechatronics, Vol. 1, No. 12, pp. 713~736. 2002
- [11] Z. Zhu and Z. Pan, "*Miniature pipe Robots*", Industrial Robot: An International Journal, Vol. 30, No. 6, pp. 575~583, 2003
- [12] I. Hayashi, N. Iwatsuki, K. Morikawa and M. Ogata, "*An in-Pipe Operation Micro robot Based on The principle of Screw*", International Symposium on Micromechatronics and Human Science, pp. 125~129, 1997.
- [13] M. Horodinca, I. Dorftei, E. Mignon and A. Preumont, "*A Simple Architecture for In-pipe Inspection Robots*", International Colloquium on Mobile and Autonomous Systems, pp. 61~64, 2002.
- [14] S. G. Roh and H. R. Choi, "*Differential-drive In-pipe Robot for Moving Inside Urban Gas Pipelines*", IEEE Transactions on Robotics, Vol. 21, No. 1, pp 1~17, 2005.
- [15] J. W. Park, T. H. Kim and H. S. Yang, "*Development of an Actively Adaptable In-pipe Robot*", IEEE International Conference on Mechatronics (ICM), 2009.

- [16] K. Suzumori, T. Miyagawa, M. Kimura and Y. Hasegawa, "*Micro Inspection Robot for 1-in Pipes*", IEEE/ASME Transactions on Mechatronics, Vol. 4, No. 3, pp. 286~292, 1999
- [17] S. Hirose, H. Ohno, T. Mitsui and K. Suyama, "*Design of In-Pipe Inspection Vehicles for $\phi 25$, $\phi 50$, $\phi 150$ Pipes*", Journal of Robotics and Mechatronics, Vol. 12, No. 3, pp. 310~317, 2000.
- [18] T. Fukuda, H. Hosokai and M. Uemura, "*Rubber Gas Actuator Driven by Hydrogen Storage Alloy for In-pipe Inspection Mobile Robot with Flexible Structure*", IEEE International Conference on Robotics and Automation, pp. 1847~1852, 1989.
- [19] S. Aoshima, T. Tsujimura and T. Yabuta, "*A Miniature Mobile Robot Using Piezo Vibration for Mobility in a Thin Tube*", Transactions of ASME, Journal of Dynamic Systems, Measurements and Control, Vol. 115, pp. 270~278, 2000.
- [20] C. Anthierens, A. Ciftci and M. Betemps, "*Design of An Electro Pneumatic Micro Robot for In-pipe Inspection*", IEEE International Symposium on Industrial Electronics, Vol. 2, pp. 968~992, 1999.
- [21] K. U. Scholl, V. Kepplin, K. Berns and R. Dillmann, "*Controlling a Multi-joint Robot for Autonomous Sewer, Inspection*", IEEE International Conference on Robotics and Automation, Vol. 2, pp. 1701~1706, 2000.
- [22] S. Wakimoto, J. Nakajima and M. Takata, "*A Micro Snake-like Robot for Small Pipe Inspection*", International Symposium on Micro Mechatronics and Human Science, pp. 303~308, 2003.
- [23] H. Borenstein, G. Granosik and M. Hansen, "*The Omni Tread Serpentine Robot for Industrial Inspection and Surveillance*",

- International Journal on Industrial Robots, Special Issue on Mobile Robots, Vol. 32, No. 2, pp. 139~148, 2005.
- [24] S. A. Zagler and F. Pfeiffer, “MORITZ, *A Pipe Crawler for Tube Junctions*”, IEEE International Conference on Robotics and Automation, pp. 2954~2960, 2003
- [25] W. Neubauer, “*A spider-like Robot That Climbs Vertically in Ducts or Pipes*”, IEEE/RSJ International Conference on Intelligent Robots and Systems, pp. 1178~1185, 1994.
- [26] W. Fischer, F. Tâche and R. Siegwart, “*Inspection System for Very thin and Fragile Surfaces, Based on a Pair of Wall Climbing Robots with Magnetic Wheels*”, IEEE/RSJ Int. Conference on Intelligent Robots and Systems, San Diego, CA, USA, pp. 1216~1221, 2007.
- [27] B. F. Yousef, N. Bastaki, N. Mavidis, S. Antail, J. Menhali, K. Al Nuami, N. Dhaheri, G. Endo, S. Hirose, H. Sekine, D. Seto, Y. Sasaki and H. Ripont, “*In-pipe Inspection Robot*”, Proceedings of the 15th International Conference on Climbing and Walking Robots and the Support Technologies for Mobile Machines, BA, USA, pp. 289 ~296, 2012.
- [28] D. W. Kim, C. H. Park, H. K. Kim and S. B. Kim, “*Force Adjustment of an Active Pipe Inspection Robot*”, ICROS-SICE International Joint Conference, 2009.
- [29] O. Tătar, D. Mândru and I. Ardelean P, “*Development of Mobile Minirobots for In pipe Inspection Tasks*”, ISSN 1392 – 1207. Mechatronika, Vol. 6, No. 2, 81~86, 2007.
- [30] Y. S. Kwon and B. J. Yi, “*Design and Motion Planning of a Two-Module Collaborative Indoor Pipeline Inspection Robot*”, IEEE Transaction on Robotics, pp. 681~696, 2012.

- [31] A. Kakogawal, T. Nishimura and S. Ma, “*Development of a Screw Drive In-pipe Robot for Passing through Bent and Branch Pipes*”, IEEE Robotics (ISR), 44th International Symposium on Robotics, 2013.
- [32] M. Ono and S. Kato, “*A Study of an Earthworm Type Inspection Robot Movable in Long Pipes*”, International Journal of Advanced Robotic Systems, Vol. 7, pp. 85~90, 2010.
- [33] A. Zagler and F. Pfeiffer, “*MORITZ a Pipe Crawler for Tube Junctions*”, Proceedings of IEEE, International Conference 2003.
- [34] J. H. Min, W. Y. Jeong, P. S. Pratama, Y. D. Setiawan and S. B. Kim, “*Fault Diagnosis System of Caterpillar Wheel Type Pipeline Inspection Robot*”, International Symposium on Mechatronics and Robotics, Vietnam, Vol. 3, pp. 74~78, 2013.
- [35] G. Hoang, J. H. Min, J. W. Kim, H. K. Kim, Y. W. Choe and S. B. Kim, “*Control of In pipe Inspection Robot in Variable Pipeline*”, International Symposium on Mechatronics and Robotics, Vietnam, pp. 55~59, 2013
- [36] H. P. Huang, J. L. Yan, and T. H. Cheng, “*Development and Fuzzy Control of a Pipe Inspection Robot*”, IEEE Transaction on Industrial Electronics, Vol. 57, No. 3, pp. 1088~1095, 2010.
- [37] Y. D. Setiawan, J. W. Kim, J. H. Min, H. K. Kim and S. B. Kim, “*Pipe Inspection Robot Controller Design Based on Linear Quadratic Regulator*”, The 7th Vietnam Conference on Mechatronics, Vietnam, pp. 493~500, 2014.

Publications and Conferences

A. Conferences

- [1] H. H. Khudhair, P. S. Pratama, H. K. Kim and S. B. Kim, “Automatic Diameter –Adjustable Controller Design of Wheel Type Pipe Inspection Robot Using Fuzzy Logic”, (ISAE 2015), Pukyong National University, Busan, South Korea, pp. 81~85, 2015.
- [2] H. H. Khudhair, P. S. Pratama¹, H. R. Yoo, D. K. Kim , V. H. Duy and S. B. Kim, “Diameter-Adjustable Controller Design of Wheel Type Pipe Inspection Robot Using Fuzzy Logic Control Method”, 3rd International Conference on Advances in Computing, Communications and Informatics (ICACCI), Vietnam pp. 789~795, 2015.